Microalgae as a novel biofactory for biocompatible and bioactive extracellular vesicles

Giorgia Adamo[1,#,*], Pamela Santonicola[2,#], Sabrina Picciotto[1,#], Paola Gargano[1], Aldo Nicosia[1], Valeria Longo[4], Noemi Aloi[4], Daniele Paolo Romancino[1], Angela Paterna[3], Estella Rao[3], Samuele Raccosta[3], Rosina Noto[3], Monica Salamone[1], Salvatore Costa[5], Caterina Di Sano[6], Giuseppina Zampi[2], Paolo Colombo[4], Mingxing Wei[7], Nicolas Touzet[8], Mauro Manno[3], Elia Di Schiavi[2,¶] and Antonella Bongiovanni[1,¶,*]

[1] Cell-Tech HUB at Institute for Research and Biomedical Innovation, National Research Council of Italy (CNR), Palermo 90146, Italy.

[2] Institute of Biosciences and BioResources , National Research Council (CNR), Naples 80131, Italy.

[3] Cell-Tech HUB at Institute of Biophysics, National Research Council of Italy (CNR), Palermo 90146, Italy.

[4] Institute for Research and Biomedical Innovation, National Research Council of Italy (CNR), Palermo 90146, Italy.

[5] Department of of Biological, Chemical and Pharmaceutical Sciences and Technologies, University of Palermo, 90128 Palermo, Italy

[6] Institute of Translational Pharmacology, National Research Council of Italy (CNR), Palermo 90146, Italy.

[7] Cellvax SAS, Villejuif Bio Park, 1 Mail du Professeur Georges Mathé, 94800 Villejuif, France.

[8] Department of Environmental Science, School of Science, Centre for Environmental Research, Innovation and Sustainability, CERIS, Atlantic Technological University Sligo, Sligo, Ireland.

[#]These first authors contributed equally to this work.

[¶]These last authors contributed equally to this work.

[*] Corresponding Authors: antonella.bongiovanni@cnr.it; giorgia.adamo@irib.cnr.it

ABSTRACT

Nanoalgosomes are extracellular vesicles (EVs) released by microalgal cells that can mediate intercellular and cross-kingdom communication. In the present study, the optimization of high quality nanoalgosome manufacturing from cultures of the marine microalgae *Tetraselmis chuii* has been enhanced by quality control procedures, applying robust biophysical and biochemical characterizations. Then, we evaluated the biological properties of nanoalgosomes in pre-clinical models. Our investigation of nanoalgosome biocompatibility included toxicological and genetic analyses, starting from studies on the invertebrate model organism *Caenorhabditis elegans* and proceeding to hematological and immunological evaluations in mice and human cells. Nanoalgosome biodistribution was evaluated in mice with accurate space-time resolution, and in *C. elegans* at cellular and subcellular levels. Further examination highlighted the antioxidant and anti-inflammatory bioactivities of nanoalgosomes. This holistic approach to nanoalgosome characterization showcases that nanoalgosomes are innate effectors for novel cosmetic formulations and EV-based therapies.

Keywords: nanoalgosomes, extracellular vesicles, exosomes, cell-free therapy, antioxidant, anti-inflammatory, biocompatibility, biodistribution, *Caenorhabditis elegans*, EV-based therapeutics.

INTRODUCTION

Among naturally occurring nanoparticles, extracellular vesicles (EVs) are membranous nanostructures secreted by nearly all cell types to transfer bioactive molecules that influence their target cells' functioning[1,2,3]. EVs exhibit good biocompatibility, low toxicity, and enhanced stability in the blood, as well as limited immunogenicity[2, 4]. Another advantage of EVs is their targeting potential: they can cross physiological barriers, such as the blood-brain barrier (BBB), and target specific cell populations[1]. Since they can carry intrinsic biological materials, EVs are currently considered one of the most promising cell-derived therapeutic effectors[5]. Furthermore, EVs may be loaded with therapeutic entities (such as small molecule drugs, nucleic acid proteins, and CRISPR/Cas9), and their endogenous cargo can enhance the effects of encapsulated drugs, creating a combinatorial effect[6,7]. In recent years, there has been growing interest in EVs derived from human mesenchymal stem cells (MSC)[8,9]. However, as MSC-EV manufacturing has turned out to be neither sustainable and controllable, nor economically and environmentally viable, the academic and industrial communities have been exploring alternative approaches to source EVs from other biological sources, such as milk, bacteria, and plants[10-14]. Among these, plant-derived vesicles are currently considered biocompatible, sustainable, and green nanocarriers for the potential development of cancer therapies[14]. In this context, our recent work has proposed microalgae as a novel, sustainable, and renewable bio-factory of EVs, to be exploited as tailor-made products for therapeutic, cosmetic, and cosmeceutical applications[15-17]. We have developed and patented a platform for the high-yield, high-quality production of EVs from microalgae, which we named "nanoalgosomes" or "algosomes"[15]. Microalgae are a heterogeneous group of eukaryotic photosynthetic autotrophs that are a rich source of bioactive metabolites, including pigments, vitamins, antioxidants, and other compounds with various health benefits (e.g., antioxidant, anti-inflammatory, and antibacterial activities)[19,20]. Microalgae also have several advantages over other EV sources, including the possibility of being grown in a scalable, cost-effective, and environmentally sustainable way in photo-bioreactors. These features all contribute to the suitability of nanoalgosomes as cosmeceutical and therapeutical ingredient.

Our previous work has shown that nanoalgosomes are small EVs (sEVs), surrounded by a lipid bilayer membrane, containing EV biomarkers and having a typical EV size distribution (about 100 nm) and density[15,16]. We focused on sEVs isolated from the marine photosynthetic chlorophyte *Tetraselmis chuii*, which is rich in vitamin E, carotenoids, chlorophyll, and tocopherols with anti-inflammatory and antioxidant properties[15, 16, 21-23]. Our

analysis showed that nanoalgosomes are non-cytotoxic and can be taken up by different cellular systems *in vitro* as well as *in vivo* by the invertebrate model organism *Caenorhabditis elegans* (Nematoda), an alternative to the mammalian model, that is faster and less expensive to use and whose body transparency is advantageous for studying nanoparticle toxicity, distribution, and uptake[24]. In addition, the current study aims to fully characterize the *in vivo* toxicity, immuno-safety, biodistribution, and bioactivity of nanoalgosomes through a multi-branched approach starting with studies on living organisms (*C. elegans* and mice) and delving into molecular mechanisms at the subcellular level. The results support the use of nanoalgosome applications not only in the pharmaceutical market but also in other sectors, including cosmetics and nutraceuticals.

RESULTS and DISCUSSION

PRODUCTION AND QUALITY CHECKING OF NANOALGOSOME PREPARATIONS

EVs are potential key players in the development of innovative treatments like cell-free therapy. Researchers have recently highlighted the advantages of using naturally occurring EVs over synthetic nanoparticles, such as their biocompatibility, biodegradability, and ability to target specific cell populations.

Our recent work aimed at setting up and optimize microalgae cultivation using photoautotrophical bioreactors and defined growth media at a batch growth regime, with biological productivity and nanoalgosome quality dependent on the species, nutrition and microclimate. We showed that nanoalgosome is a new type of EV with biophysical and biochemical properties as outlined in the MISEV guidelines, specifically applied to nanoalgosomes[15]. Further, the isolation efficiency of differential ultracentrifugation and tangential flow filtration (dUC and TFF) has been tested[15]. dUC was elected as the small-scale isolation method for microalgal EVs[15,16]. For larger scale processes (up to 7 L), TFF was more feasible[16] and then applied in the present study. Here, physicochemical features have been analyzed in-depth to evaluate nanoalgosome quality and yield, in each nanoalgosome preparation used in the present studies (Figure 1, upper panel). Multiple orthogonal physical and molecular techniques have been applied, including Nanoparticle Tracking Analyses (NTA), Dynamic Light Scattering (DLS), Atomic Force Microscopy (AFM), microBCA, SDS-PAGE and Western blot, also, membrane-labelling using specific fluorescent dyes and validations with fluorescent-nanoparticle tracking analysis (F-NTA) was performed (Figure 1, lower panel). Our results confirmed the presence of sEVs in the microalgal-conditioned media, with expected average diameter (e.g., 100$\pm$10 nm measured by NTA and DLS), morphology, EV markers (*e.g.*, Alix, H^+-ATPase and enolase positivity) and total EV protein/particle number ratio (*e.g.*, 1 µg of total EV protein corresponds to a range of 5-10x10^9 in all nanoalgosome batches, n=6), showing that the variability of the input material is minimized. All these features grant high batch-to-batch consistency and quality, and repeatedly yielding vesicles (~10^{12} nanoalgosomes/L of microalgal conditioned-medium, corresponding to ~10^9 nanoalgosomes/mg of dried microalgal biomass) with stable biophysical and biochemical properties.

Our previous study on nanoalgosomes showed that they are highly stable in human blood plasma, non-cytotoxic *in vitro* and can be taken up by various cellular systems[15,24]. Here, to fully characterize the compatibility, distribution, and bioactivity of nanoalgosomes, we

conducted a comprehensive analysis both *in vivo,* using *Caenorhabditis elegans* and mice, *in vitro* with human cell lines, and *ex vivo* with human basophils from whole blood.

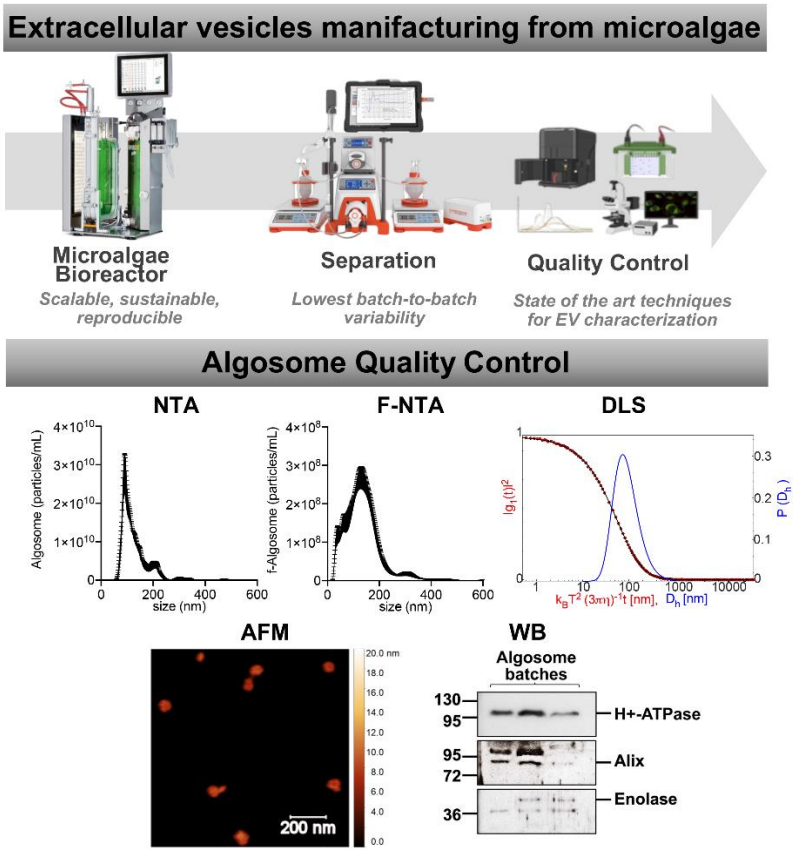

Figure 1. The production and characterization workflow of nanoalgosomes. To produce the nanoalgosomes, *Tetraselmis chuii* microalgal cells grown in photobioreactors, under controlled conditions, and the conditioned media underwent TFF separation and diafiltration (upper panel). The particle size and concentration of the nanoalgosome preparations were determined by NTA, F-NTA and DLS. Morphology of nanoalgosomes was analyzed by AFM. SDS-PAGE Western blot analyses were performed on three different nanoalgosome batches to detect the markers H^+-ATPase, Alix and enolase. Representative results of three independent biological replicates (lower panel).

NANOALGOSOME BIOCOMPATIBILITY *IN VIVO, EX VIVO* AND *IN VITRO*

In vivo biocompatibility of nanoalgosomes in C. elegans

For *in vivo* analyses of nanoalgosome biocompatibility, we firstly used the model system *C. elegans* which is highly recommended for toxicological studies since it raises fewer ethical concerns, is less expensive, and faster to use than higher level model organisms, thus reducing the number of vertebrate animals used. *C. elegans* offers a comprehensive set of experiments that allow the evaluation, in a whole living animal, of the putative toxic effect of nanoparticles on animal survival, growth, lifespan, fertility, lethality, and neuron viability, among others. After quality checks on the nanoalgosome batches (Figure 1), we treated

wild-type animals through *in liquido* culturing for 72 hours with increasing concentrations of nanoalgosomes (1, 20, 64, 128 µg/mL), first evaluating animal viability and capability of reaching adulthood. These concentrations were chosen because we had previously demonstrated that nanoalgosomes are successfully taken up by *C. elegans* at 20 µg/mL[24]. After treatment for 4 days *in liquido,* we did not observe any toxic effect of nanoalgosomes, as all the animals were alive and reached adulthood, similarly to the animals treated with mock (Figure 2a and b). Thereafter, we decided to use the concentration of 20 µg/mL to further evaluate nanoalgosome effects on animal fitness[25]. *C. elegans*' development and growth are finely regulated in four larval stages followed by a fertile adult stage, which can be altered when the animals are exposed to toxic agents[26]. To evaluate animal growth, we treated animals chronically with nanoalgosomes and tested the percentage of animals at each developmental stage every 24 hours, without observing any alterations or delays compared to animals treated with PBS as mock (Figure 2c). We also treated animals over their entire lifespan and, also in this case, nanoalgosomes had no effect on their survival curve (Figure 2d).

Another aspect used to assess the biocompatibility of nanoparticles is to evaluate their effects on animal fertility and offspring survival. Therefore, after chronic treatment of animals from eggs to L4 larval stage, we assessed the animals' egg-laying ability and egg hatching (Figure 2e and f), without observing any effects of nanoalgosome treatment compared to mock. This result confirms that nanoalgosomes do not affect animal fertility, offspring release, or embryonic survival. Moreover, we decided to evaluate the putative neurotoxicity of nanoalgosomes. *C. elegans*' transparency makes it possible to observe specific cell types, such as neurons, in living animals by using fluorescent proteins that are only expressed in the cells of interest. We thus evaluated the effects of nanoalgosomes on three different neuronal classes: GABAergic motoneurons, dopaminergic sensory neurons, and glutamatergic mechanosensory neurons. Interestingly, the invariant cell lineage in *C. elegans* determines a fixed number of neurons in adults, with 19 GABAergic motoneurons in the ventral cord, 6 dopaminergic neurons in the head, and 6 mechanosensory neurons along the body. Chronic treatment with nanoalgosomes did not cause any degeneration of the neurons analyzed (Figure 2g-i; Supporting Figure 1a-c) as the number of visible neurons was not affected by the treatment. Moreover, all these neurons exhibited normal morphology. Taken together, our results demonstrate that nanoalgosomes are very well tolerated *in vivo* by *C. elegans*, and no toxicity was observed after chronic exposure at these concentrations.

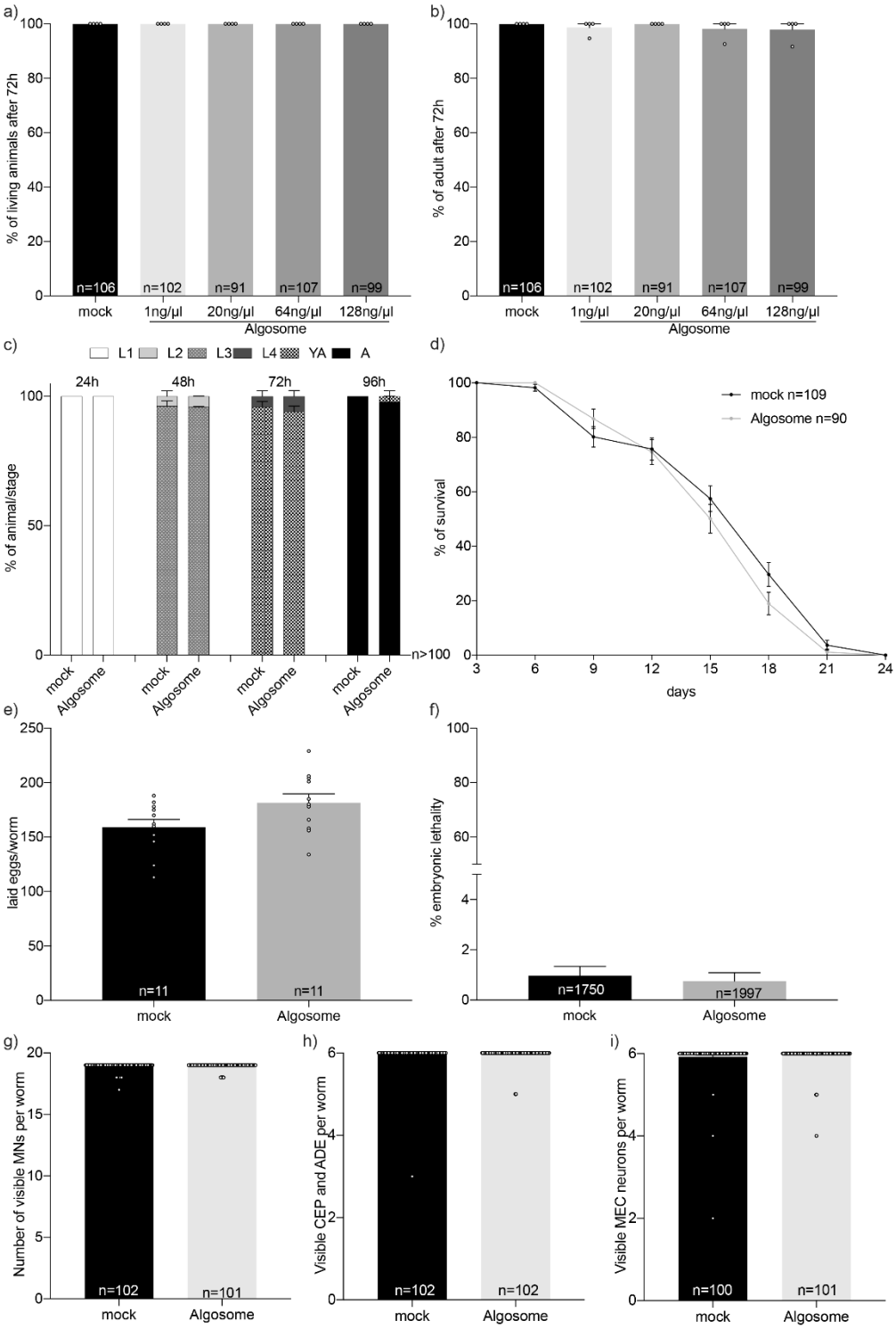

Figure 2. **Nanoalgosome *in vivo* biocompatibility in *C. elegans*.** **a)** Quantification of the number of living animals after treatment with (PBS) mock or different nanoalgosome concentrations. **b)** Quantification of the number of animals reaching adult stage after treatment with mock or different nanoalgosome concentrations. **c)** Quantification of the percentages of animals at each developmental stage after treatment with mock and nanoalgosomes (20 µg/mL). **d)** Lifespan of animals treated with mock and nanoalgosomes (20 µg/mL). **e)** Brood size of animals after treatment with mock and nanoalgosomes (20 µg/mL). **f)** Embryonic lethality of animals after treatment with mock and nanoalgosomes (20 µg/mL). **g-i)** Quantification of the number of visible motoneurons (MNs), dopaminergic neurons in the head (CEP and ADE) and mechanosensory neurons (MEC)

after treatment with mock and nanoalgosomes (20 µg/mL). Bars represent the means and dots replicates (in a-d, f-i) or single animals (in e); error bars are SEM. n is the number of animals analyzed (in a-d, i), the number of P0 animals (in e), or the number of eggs analyzed (f). In all graphs the statistical significance of the differences between treatments with mock and nanoalgosomes was assessed with Kruskal-Wallis One-way ANOVA (a-b), non-parametric Compare two proportions test (c), Mann Whitney *t-test* (e-i) or Log-rank (Mantel-Cox) test (d) and never found significant ($p>0.05$).

In vivo biocompatibility of nanoalgosomes in wild-type mice

Furthermore, biochemical and hematological studies were conducted on wild-type BALB/c mice to thoroughly evaluate the *in vivo* biocompatibility of nanoalgosomes in immune-competent mice, after a single intravenous (I.V.) administration of nanoalgosome. Wild-type BALB/c mice (n=4, 2 male and 2 female) were injected with nanoalgosomes and a free dye negative control, via the intra-ocular vein. Blood samples were collected from two mice (1 male, 1 female) at 4 time points (3, 6, 24, 48 h) to analyze hematocrit, creatinine, blood urea nitrogen (BUN), liver transaminase enzymes (Serum Aspartate Transaminase, AST, and Serum Alanine Transaminase, ALT), and lymphocyte numbers. The starting nanoalgosome doses were based on literature; in different pre-clinical studies the dose of EVs per kg of body weight ranged from 0.10 to 100 mg of total EV proteins, with an average of 2.75 mg/kg[27-29]. Based on the estimation that the body weight of 6-week-old BALB/c mouse is approximately 20 grams, the average I.V. dose of EVs in mice corresponds to 55 µg/mouse[30,31]. Thus, in our pre-clinical studies we used the following doses: Dose 1 (low dose) = 10 µg, corresponding to $4x10^{10}$ EVs/mouse; Dose 2 (high dose) = 50 µg, corresponding to $2x10^{11}$ EVs/mouse. Table 1 shows no changes in total white blood cells compared to the normal range, and no alterations in red blood cell counts, hemoglobin, or hematocrit were observed. Further, creatinine, urea and BUN, as well as AST and ALT values were similar to the control group, indicating normal kidney and liver functions. These results suggest that nanoalgosomes did not exhibit toxic effects, blood parameter alterations, or early immune response activation after a single acute I.V. administration. The effects of nanoalgosomes in mice were also evaluated through clinical signs, body weight, and visual observations. Daily clinical examinations were performed to check behavior and signs of suffering, such as cachexia, weakness, and difficulty moving or feeding, and compound toxicity, like hunching and convulsions. Supporting Table 1 shows that there was not significant body weight loss, indicating that nanoalgosome administration was well-tolerated by the animals. Our results demonstrate that a single dose of up to $2x10^{11}$ nanoalgosomes per mouse did not elicit any noticeable immune response or local and

systemic toxicity in immune-competent BALB/c mice, allowing for dose escalation or repeated administrations. This is in line with our *C. elegans* results and with previously published data on I.V. administration in mice of xenogenic milk-, human- and plant-derived EVs[4,32,33]. However, additional safety evaluations are necessary, since it is important to further expand *in vivo* studies on nanoalgosome tolerability with repeated administration in mice and larger animals, along with bio-distribution information to fully understand the potential and future applications[29].

Table 1. Hematological and biochemical analyses of peripheral blood from BALB/c mice after ocular I.V. injection of nanoalgosomes after 48h.

Parameters	Dose 1	Dose 2	Control
Hematological			
Red blood cells ($x10^6$/µL)	10.1 ± 0.0	9.9 ± 1.0	10.1 ± 0.1
Hemoglobin (g/dL)	15.2 ± 0.0	15.0 ± 1.4	15.5 ± 0.5
MCV (fL)	47.0 ± 0.2	45.5 ± 0.5	47.5 ± 0.5
Hematocrit (%)	47.0 ± 0.2	46.0 ± 5.0	48.0 ± 1.0
Reticulocytes (%)	3.4 ± 0.1	2.1 ± 0.0	2.2 ± 0.3
MCH (pg)	15.0 ± 0.0	15.0 ± 0.0	15.5 ± 0.5
Leukocytes ($x10^3$/µL)	3.1 ± 0.0	3.1 ± 2.0	4.8 ± 0.9
Lymphocytes (%)	72.0 ± 0.3	67.0 ± 2.0	78.0 ± 2.0
Neutrophils (%)	20.0 ± 0.1	25.0 ± 1.0	16.0 ± 2.0
Monocytes (%)	2.0 ± 0.0	3.0 ± 1.0	1.5 ± 0.5
Eosinophils (%)	3.0 ± 0.0	3.4 ± 0.5	2.5 ± 0.5
Basophils (%)	0.0 ± 0.0	0.5 ± 0.0	0.5 ± 0.0
Biochemical			
Creatinine (mg/L)	4.0 ± 0.0	4.0 ± 0.8	4.2 ± 0.4
BUN (mg/dL)	23.0 ± 5.7	20.6 ± 6.6	27.0 ± 2.2
Urea (g/L)	0.5 ± 0.1	0.4 ± 0.1	0.5 ± 0.0
ALT ($x10^3$ UI/L)	2.8 ± 1.5	2.6 ± 0.4	2.1 ± 0.4
AST ($x10^3$UI/L)	2.5 ± 0.6	4.0 ± 0.6	3.4 ± 0.3

Immune-compatibility assessment ex vivo

To verify the absence of potential immune-reaction to nanoalgosomes, we performed an *ex vivo* basophil activation test using whole blood from healthy subjects (n=3). A specific monoclonal antibody (anti-FcεRI) binding to the high affinity IgE binding receptor was used as positive control. Flow cytometry characterization showed no basophil activation following nanoalgosome treatments at different doses (0.25-2 µg/mL), with a percentage of basophil activation similar to the negative control (Figure 3; Supporting Table 2).

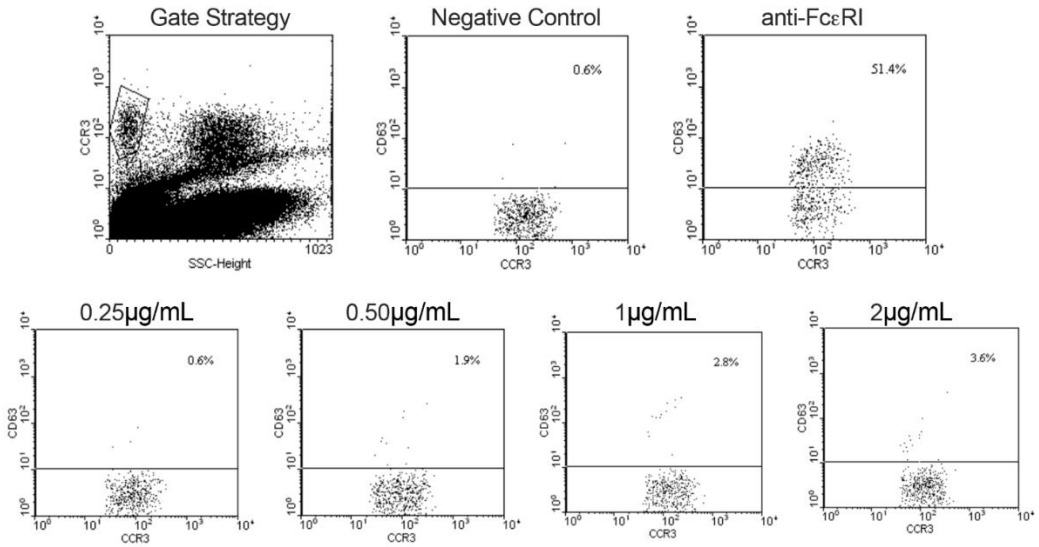

Figure 3. **Flow cytometry-based basophil activation test.** Upper panels indicate: a representative gate strategy used to select the CCR3 and CD63 populations, negative, and positive (Anti-FcƐRI) controls. Bottom panels show the activation induced by different concentrations of nanoalgosomes. Representative results of three independent biological replicates are shown.

Genotoxicity assessment in vitro and in vivo

To evaluate nanoalgosomes' potential as therapeutic effectors, a comprehensive preclinical study delving even deeper into the molecular level was crucial. Our group recently demonstrated that nanoalgosomes did not elicit cytotoxicity, hepatotoxicity or genotoxicity in different cell lines[15,16]. Here, we have examined whether nanoalgosome treatment could trigger the activation of DNA-damage pathways by conducting gene expression analysis in 1-7 HB2 normal mammary epithelial cells. Typically, DNA damage leads to cell cycle arrest, regulation of DNA replication, and activation of the repair pathway. DNA damage triggers the activation of DNA-damage sensors such as *ATR* (ATM and Rad3-related serine/threonine kinase) and their recruitment to DNA damage sites[34,35]. In addition, *checkpoint kinase 1* (*CHEK1*) is a key downstream molecule of DNA-damage response signaling; CHEK1 phosphorylates various intracellular substrate proteins, including the RAD51 recombinase which is central to the homologous recombination pathway, and binds single-stranded DNA at damage sites, forming filaments observed microscopically as nuclear foci. Therefore, these genes are considered to be involved in the response to DNA damage maintaining genome integrity, with *ATR* initiating a signaling cascade that activates *CHEK1* and *RAD51*[36-38]. Gene expression analysis of 1-7 HB2 cells treated with 2 µg/mL of nanoalgosomes for 24 hours showed not significant changes in the expression level of DNA-damage sensors (*ATR*, *CHECK1*, *RAD51*), thus suggesting that the outcomes related to

nanoalgosomes are negligible on the activation of the DNA damage signaling pathway (Figure 4a).

The *C. elegans* germline can be used as a tool to study genotoxicity *in vivo*[39]. In fact, genotoxic agents, such as doxorubicin[40], are capable of increasing physiological germline apoptosis. An average of three apoptotic corpses per gonadal arm can be visualized using SYTO12, an apoptotic-DNA fluorescent marker, in the wild-type[41,42]. After chronic treatment of animals with nanoalgosomes at 20 µg/mL we did not observe any increase in the number of apoptotic corpses in the germline compared to mock (Figure 4 b). Differently, animals treated with doxorubicin showed a higher number of apoptotic corpses compared to animals treated with mock, thus confirming that nanoalgosomes have no genotoxic effect at the concentration tested neither *in vitro* nor *in vivo*.

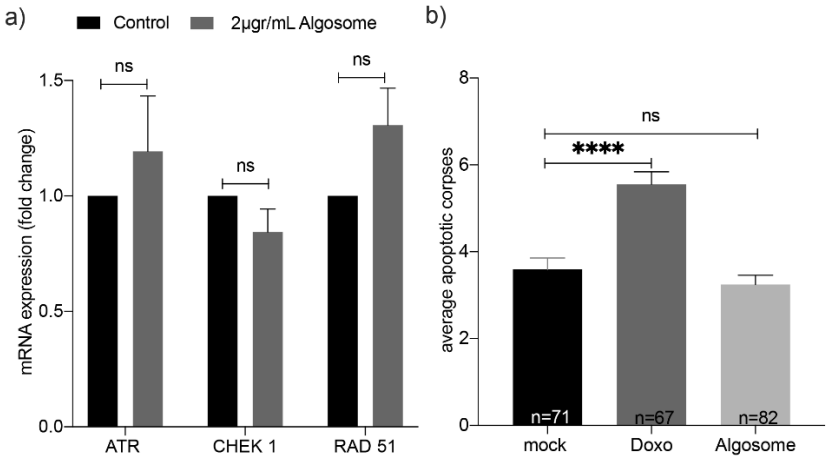

Figure 4. **Genotoxicity assessment *in vitro* and *in vivo*. A)** Real-time PCR for quantification of DNA-damage sensors expression levels following exposure to nanoalgosomes (2 µg/mL for 24h in 1-7 HB2 cells). Fold-changes were normalized with β-actin expression and given as relative to control. Each experiment was performed in triplicate. By One-way ANOVA differences of treated cells were determined not statistically significant when compared with the control ($p>0.05$). **B)** Quantification of SYTO 12 positive apoptotic corpses in the germline after treatment with mock (PBS), Doxo (doxorubicin 2.4 µM), and nanoalgosomes (20 µg/mL). Bars represent means; error bar is the SEM. n is the number of animals analyzed. Kruskal-Wallis one-way ANOVA was used to assess the statistical significance of the differences: mock vs nanoalgosomes ns, $p=0.7870$; mock vs Doxo****, $p<0.0001$.

Biodistribution of nanoalgosomes in nude mice

Due to their lipophilic nature, EVs can be labeled with fluorescent lipid dyes and their biodistribution as well as pharmacokinetics has been evaluated in pre-clinical studies mainly using mouse models and recently using larger animals, including the pig-tailed macaque (*Macaca nemestrina*)[29, 43, 44]. To assess the biodistribution of nanoalgosomes systemically delivered in mice, the near-infrared dye DiR was used for nanoalgosome labeling. DiR is a

lipophilic dye that fluoresces intensely only when inserted into a lipid membrane. The fluorescence spectrum of this dye (emission peak of 790 nm) allows for efficient penetration through bones and tissues with low autofluorescence, making it ideal for imaging in living animals. Nanoalgosomes were labeled with the DiR probe, while the same amount of DiR diluted in PBS was used as a free dye control. Both samples underwent NTA analysis after the removal of the free dye by ultracentrifugation and extensive washing steps. The NTA data showed a typical nanoalgosome size distribution with a mode size of 100 nm in diameter (Supporting Figure 2a). The presence of DiR-fluorescence in the nanoalgosome-labeled samples was verified by IR measurements using an Odyssey scanner, while for the free dye control, no fluorescence signal was detected (Supporting Figure 2b). Athymic nude mice (n=6; 3 male, 3 female) were injected with aforementioned DiR-labeled nanoalgosomes at two doses (or the same volume of the free dye control) via the intra-ocular vein. The biodistribution of the DiR-labeled nanoalgosomes was examined in live animals using IVIS Spectrum Imaging. Mouse backs (male, prone in Figure 5a, b, c; female prone in Supporting Figure 3a) and stomachs (male, supine in Supporting Figure 3b) were imaged at 3, 6, 24 and 48 hours post-IV injection. At 3 hours post-injection, the DiR-nanoalgosome fluorescent signals were circulating in the bloodstream and disseminating throughout the animals' bodies, accumulating mainly in the liver. Fluorescent signals increased in a time- and dose-dependent manner, as shown in the total radiant efficiency plot (Figure 5d). In contrast, lower and more constant fluorescent background signals were detected for the free dye control-treated mice after each imaging, highlighting the specificity of the DiR-nanoalgosome signal. Interestingly, nanoalgosome localization (dose 2, Figure 5c) was more evident in bones, the spine, and the thymus after 24 and 48 hours. The fluorescence levels of DiR-nanoalgosome signals in two target areas (liver and femur) were quantified at each time point using IVIS software. As shown in Figure 5e and f, nanoalgosomes were mainly localized in the liver 3 hours post-injection (as commonly observed for other EVs) and their concentration significantly decreased over time. Meanwhile, their concentration increased and significantly accumulated in bones (femur) by 48 hours. This organotropism is peculiar for nanoalgosomes, as most mouse studies with MSC-derived EVs have reported that EVs accumulate to the liver, spleen, and sometimes kidney and lung, with rapid clearance from blood circulation after systemic injection[27, 28,43, 44].

Our data suggest a very high stability of nanoalgosomes in circulation and a specific organotropism for bone compartments. The increasing fluorescent signals for up to 48 hours

in mice and in individual areas (*e.g.*, femur) suggests that nanoalgosomes are stable in bodily fluids and that their circulating half-life is high.

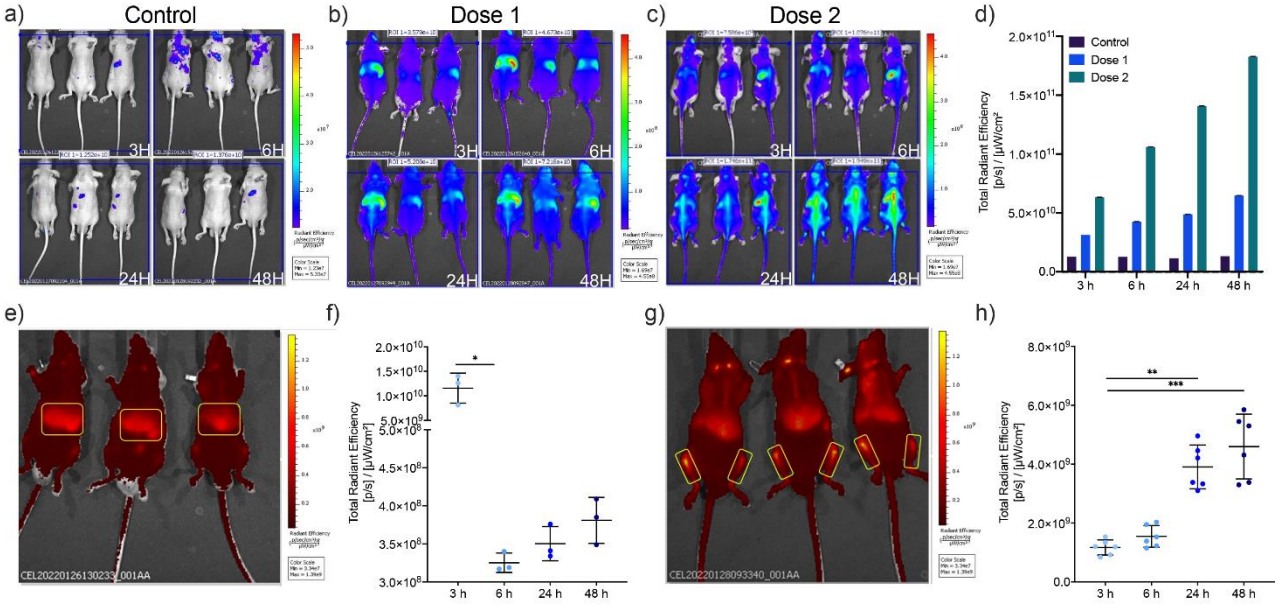

Figure 5. **IVIS imaging of DiR-labeled nanoalgosome biodistribution in nude mice after IV injection.** Nude mice (n=3; male, prone) were injected with (a) v/v of free dye control /200 µL/mouse; (b) dose 1: 10µg nanoalgosomes/200 µL/mouse; (c) dose 2: 50µg nanoalgosomes/200 µL/mouse and control. Nanoalgosome biodistribution was measured at 3, 6, 24 and 48h post-injection using an IVIS *in vivo* imaging system at ex/em 644/665. d) Total radiant efficiency plot of DiR-labeled nanoalgosomes (doses 1 and 2) and the free dye control 3, 6, 24 and 48h post-injection. e-f) Representative images of DiR-nanoalgososome fluorescence in the liver (3h post I.V.) and respective radiance efficiency quantification graph at 3, 6, 24 and 48h. Kruskal-Wallis one-way ANOVA was used to assess the statistical significance of the differences: 3h vs 6h*, $p<0.05$. g-h). Representative images of DiR-nanoalgososome fluorescence in the femur (48h post I.V.) and respective radiance efficiency quantification graph at 3, 6, 24 and 48h. Kruskal-Wallis one-way ANOVA was used to assess the statistical significance of the differences: 3h vs 24h**, $p<0.01$; 3h vs 48h***, $p<0.001$.

NANOALGOSOME INTERNALIZATION MECHANISM AND INTRACELLULAR LOCALIZATION

In our previous study, we demonstrated that nanoalgosomes, when labeled with Di-8-ANEPPS, PKH26, or DiR, are taken up and localized *in vitro* in the cytoplasm of cells and *in vivo* in the cytoplasm of *C. elegans* intestinal cells[15,24]. Therefore, we investigated the molecular mechanisms involved in nanoalgosome internalization *in vitro* and *in vivo*. Since we proved that nanoalgosomes are internalized within human cells in a dose- and time-dependent manner through an energy-dependent mechanism, we hypothesized multiple endocytic pathways, including micropinocytosis, clathrin- and caveolae-mediated endocytosis, as possible mechanisms of nanoalgosome internalization that were reported

for other EVs[45]. To test among these alternative hypotheses, we used three specific blocking agents in 1-7 HB2 cells: dynasore to inhibit clathrin-mediated endocytosis, nystatin to interfere with caveolae-dependent uptake, and EIPA to inhibit micropinocytosis[45-49]. We monitored intracellular nanoalgosome uptake in cells by measuring the fluorescence intensity of Di-8-ANEPPS-labeled nanoalgosomes after 2 and 3 hours of incubation with nanoalgosomes, with or without inhibitors (Figure 6a, Supporting Figure 4). The results showed that cells treated with dynasore (60µM) had a nanoalgosome internalization trend similar to the negative control (*i.e.,* cells incubated at 4°C, that are inhibited for all energy-dependent processes), thus indicating that dynasore inhibited nanoalgosome cellular uptake. In contrast, no significant endocytosis inhibition was observed in cells treated with EIPA (10µM) or nystatin (50µM), which showed a nanoalgosome internalization level similar to the positive control (*i.e.*, cells incubated at 37°C). Cell are viable for each treatment, demonstrating that none of the inhibitors used, at any concentration, were toxic to the cells (Supporting Figure 4a). These results indicate that clathrin-dependent endocytosis plays a role in the cellular uptake of nanoalgosomes. To confirm the results obtained *in vitro,* we took advantage of the ease in *C. elegans* to use genetic mutants and dissect molecular pathways. In particular, when the clathrin heavy chain gene is mutated in *C. elegans*, the uptake of nanoparticles is impaired[50]. Thus, we used a *KO* mutant in the clathrin heavy chain, *chc-1(ok2369*), and since *chc-1* is an essential gene and its depletion causes animal lethality, we analyzed heterozygous balanced animals (*chc-1 KO/*+). We treated for 24 hours animals with nanoalgosome fluorescently labelled with Di-8-Anepps and observed, in wild-type animals, a fluorescent signal in the intestinal cells (Figure 6b, left panel). On the contrary, in all *chc-1 KO/*+ animals analyzed, the fluorescent signal in the intestinal cells was strongly reduced (Figure 6b, right panel). Our results demonstrate that nanoalgosome are actively internalized *in vitro* and *in vivo* by clathrin-mediated endocytosis.

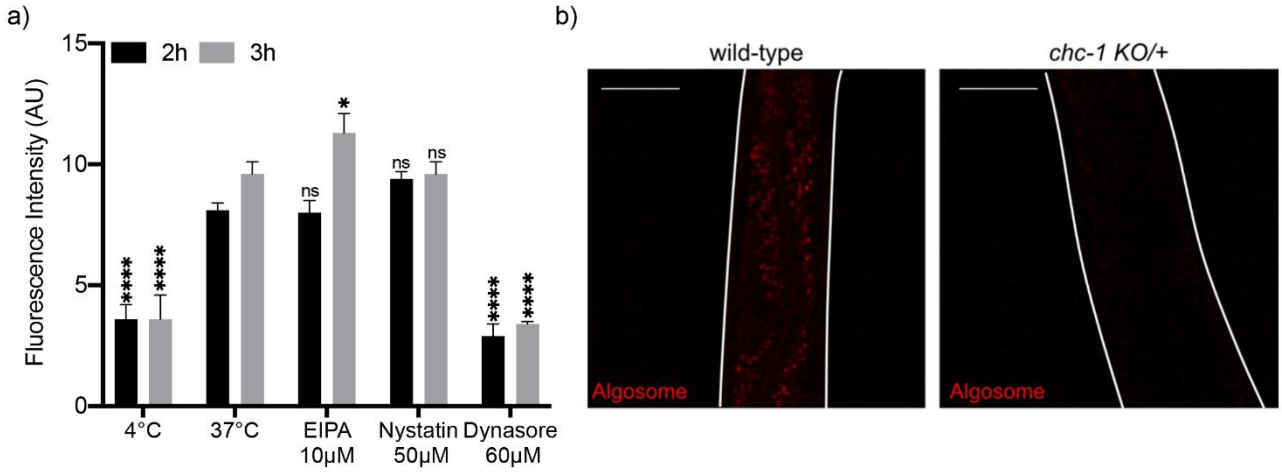

Figure 6. **Molecular mechanism of nanoalgosome internalization in human cell lines and *in vivo*. a)** Effect of metabolic inhibitors of endocytosis on nanoalgosome uptake in 1-7 HB2 cells treated with nystatin, EIPA and dynasore. Results are presented as arbitrary unit of nanoalgosome fluorescence intensity inside cells after 2 and 3h of incubation. Each value represents the mean ± SD from three independent experiments. One-way ANOVA statistical test was used to assess the statistical significance of the differences: 37°C (2h) (3h) vs 4°C (2h) (3h), EIPA 10 µM (2h) (3h), nystatin 50 µM (2h) (3h) and dynasore 60 µM (2h) (3h), ****p<0,0001, ns=not significant. **b)** Representative confocal images of wild-type (left), *chc-1 KO* (right) heterozygote animals after 24h of treatment with Di-8-Anepps labelled nanoalgosomes (red). Fluorescent signal is observed only in the intestinal cells of wild-type animals, while in *chc-1 KO* heterozygote animals the fluorescent signal is strongly reduced. Animal body is outlined with white lines. Scale bar is 50 µm.

We further investigated the subcellular fate of labeled nanoalgosomes once internalized, both *in vitro* and *in vivo*. The *in vitro* subcellular localization of PKH26-labeled nanoalgosomes was determined using immunofluorescence and confocal microscopy (Figure 7a). Three distinct subcellular compartments were evaluated for *in vitro* study: the endosomal compartment, the lysosomal system, and the endoplasmic reticulum (ER), using established biomarkers (CD63, LAMP1, and Calnexin, respectively).

After 24 hours of incubation, we found a co-localization of nanoalgosomes (red signal) with the endosomal protein CD63 (green signal). Fluorescence images (Supporting Figure 5) showed this co-localization in a large portion of the cells, suggesting involvement in endosomal compartments. Confocal images (Figure 7a) further confirmed this direct relation with the endosomal system in the area where the fluorescence appears yellow.

Furthermore, the localization of PKH26-labeled nanoalgosomes was evaluated in relation to two other intracellular markers, LAMP-1 and calnexin. Both fluorescence and confocal images showed that intracellular LAMP-1-positive compartments (green) did not co-localize with internalized PKH26-labeled vesicles, suggesting that lysosomes were not involved in

their intracellular trafficking. A possible connection with the ER in nanoalgosome trafficking was also observed by examining the localization of the calnexin protein. In this case, however, the green signal of calnexin-positive regions and red vesicles inside cells showed different localization, excluding the ER from the intracellular nanoalgosome pathway.

To confirm these observations *in vivo*, we took advantage of *C. elegans*' transparency and transgenic expression of fluorescent proteins in the Golgi (GFP fused to AMAN-2 protein) or late endosomes (GFP fused to RAB-7 protein). AMAN-2 is a membrane protein of the Golgi, and we did not observe any co-localization with Di-8-ANEPPS-labeled nanoalgosomes, as shown in Figure 7b (upper panels). On the other hand, when we used a marker for late endosome membranes (RAB-7), we observed the nanoalgosome fluorescent signal inside the endosomes (Figure 7b, lower panels). Taken together, our results suggest that after nanoalgosomes are internalized by clathrin-mediated endocytosis, the fluorescent signal of nanoalgosome membrane co-localizes only with the endosome and not with the lysosomes, thus suggesting that nanoalgosomes are not destined to lysosomal degradation. These data also demonstrate that nanoalgosome internalization mechanisms are conserved across species.

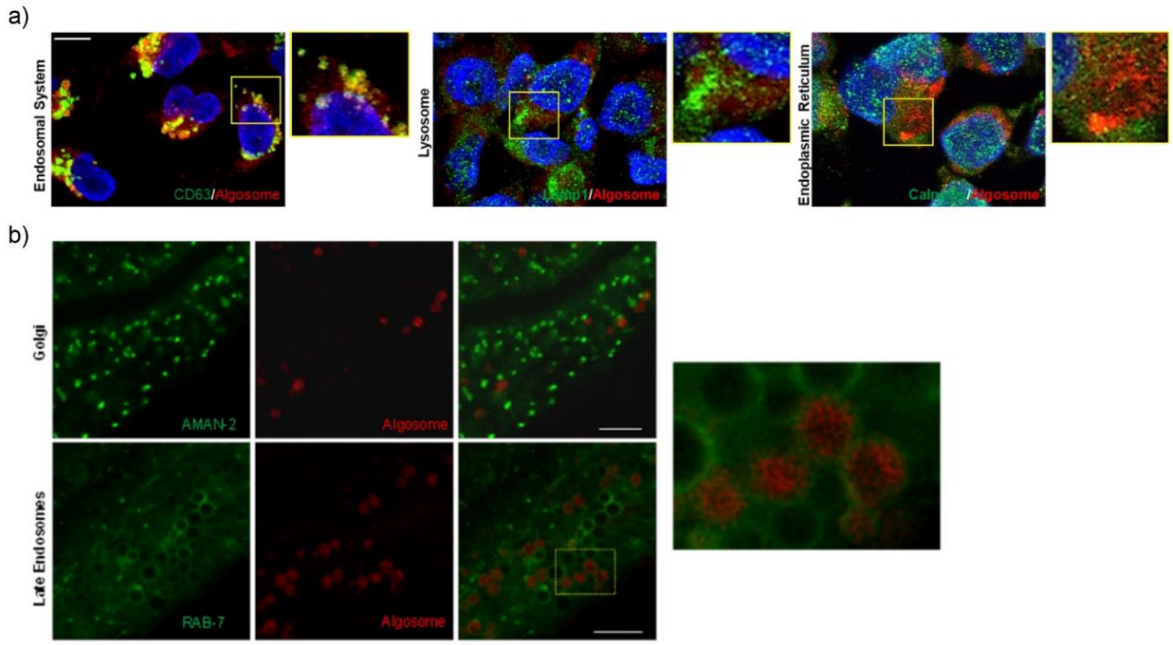

Figure 7. **Intracellular nanoalgosome localization. a)** Confocal microscopy analyses *in vitro.* In green are the endosomal system (CD63), the endoplasmic reticulum (Calnexin) and lysosomes (Lamp1) of MDA MB 231 cells, incubated with PKH26-labelled nanoalgosomes (red) for 24h. Scale Bar are 50µm. **b)** Confocal microscopy analysis of *C. elegans* intestinal cells. In green the Golgi marker AMAN-2 (upper panels) and late endosomes marker RAB-7 (lower panels). In red Di-8-Anepps labelled nanoalgosomes. Scale bar 25 µm. An enlargement of the yellow box is visible on the right.

NANOALGOSOME BIOACTIVITY *IN VITRO* AND *IN VIVO*

Antioxidant activity of nanoalgosomes

Microalgae are sources of antioxidant compounds[51,52], so we sought to determine the potential antioxidant role of microalgae-derived EVs. Nanoalgosome antioxidant activity was evaluated in two different cell lines: tumoral (MDA-MB 231) and normal (1-7 HB2), using the cell-permeable DCF-DA fluorescent probe that emits fluorescence proportionally to intracellular ROS content. Oxidative stress was induced using H_2O_2 (Supporting Figure 6a) and tert-butylhydroperoxide (TBH), which are oxidant agents that increase intracellular ROS levels. Cell viability analyses showed that none of the concentrations of the oxidant agents used were toxic to the cells (Supporting Figure 6b, c). Figure 8a shows the percentage of ROS levels in cells treated with different nanoalgosome concentrations (0.5, 1, and 2 µg/mL) for 24 hours, with and without oxidative stress induction. As shown, treatments with nanoalgosomes did not induce oxidative stress, and the percentage of ROS levels was comparable to the negative control (untreated cells). After treatment with oxidant agents, ROS levels significantly increased in both cell lines. However, these increases in ROS levels were significantly lower in stressed cells which had been pre-treated with nanoalgosomes for 24 hours, suggesting that nanoalgosomes significantly reduced ROS levels and rebalanced the physiological ROS levels in both cell lines.

To further investigate the antioxidant abilities of nanoalgosomes, we analyzed whether they could counteract ROS, directly or indirectly modulating the expression of oxidative stress responsive genes. We selected a panel of genes that play important roles in regulating oxidative stress and maintaining cellular homeostasis. For instance, *AKR1C2* (aldo-keto reductase family 1 member C2) plays a role in detoxifying lipid peroxidation products, which can contribute to the production of ROS. *FTH1* (ferritin heavy chain1) helps to regulate iron levels, which is important for ROS regulation since iron can catalyze the production of free radicals. *Alox12* (arachidonate 12-Lipoxygenase) can contribute to oxidative stress by producing leukotrienes, which are inflammatory mediators that can increase ROS production. *NOS2* (nitric oxide synthase) produces nitric oxide, which can have harmful effects on oxidative stress. Further, to counteract the effects of ROS, *CAT*, *GPX1* and *GSR* (catalase, glutathione peroxidase and reductase, respectively) work to neutralize ROS by converting them into less harmful products and to maintain the redox balance by reducing glutathione disulfide, which can be formed as a result of ROS exposure[53]. Thus, these genes and their products are interconnected and work together to regulate ROS levels in cells and maintain cellular homeostasis. After incubating 1-7 HB2 cells with 2 µg/mL of

nanoalgosomes for 24 hours, with and without oxidant agent treatment, real-time PCR analyses were carried out to evaluate the mRNA expression levels of the defined genes involved in the oxidative stress cellular signaling (Figure 8b, c, d). The results showed that the expression of oxidative stress-related genes in cells treated with nanoalgosomes for 24 hours was similar to that of untreated cells, confirming that nanoalgosomes did not induce expression alterations of genes related to oxidative stress.

As expected, after oxidative stress induction, these genes were upregulated, while interestingly the expression levels of most of the genes analyzed were significantly re-established or lowered in stressed cells pre-treated for 24 hours with nanoalgosomes. These results suggested that microalgal-derived EVs have potent antioxidant abilities, likely due to their antioxidant cargo and ability to neutralize free radicals, promoting protective mechanisms inside cells.

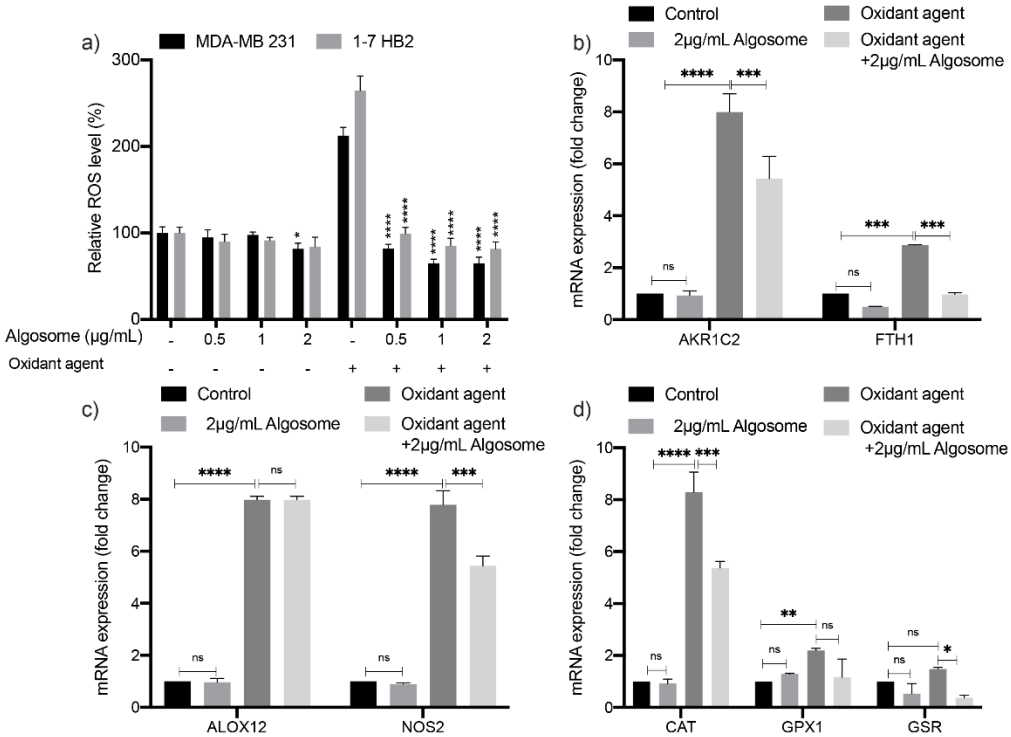

Figure 8. **Antioxidant bioactivity of nanoalgosomes in model cellular systems. a)** Percentage of ROS production in 1-7 HB2 and MDA MB 231 cells treated with nanoalgosomes (0.5-1-2 µg/mL) for 24h, with/without oxidant agent (250 µM TBH), normalized to untreated cells. Values are means ± SEM of three independent experiments. One-way ANOVA was used to assess the statistical significance of the differences: MDA-MB 231 vs MDA-MB 231 2 µg/mL nanoalgosome, *p<0.05; 1-7HB2 vs 1-7HB2 2µg/mL nanoalgosome, *p<0.05; MDA-MB 231 + oxidant agent vs MDA-MB 231 0.5-1-2 µg/mL nanoalgosome + oxidant agent, ****p<0.0001; 1-7HB2 + oxidant agent vs 1-7HB2 0.5-1-2 µg/mL nanoalgosome + oxidant agent, ****p<0.0001**. b-d)** Real-time PCR quantification of antioxidant enzyme expression levels after exposure to nanoalgosomes (2 µg/mL) for 24h, with/without oxidant agent (250 µM H_2O_2) in 1-7 HB2 cells. Each experiment was performed in triplicate. Three-way ANOVA statistical test was used to assess the statistical significance of the differences:

Control vs 2 µg/mL algosome; Control vs Oxidant agent; Oxidant agent vs Oxidant agent + 2 µg/mL algosome, *p<0.05, **p<0.01,***p<0.001, ****p<0.0001, ns=not significant.

To validate the nanoalgosome antioxidant effect *in vivo*, we evaluated the response of treated *C. elegans* animals to exogenous oxidative stress. Acute treatment of *C. elegans* with H_2O_2 can induce a nearly complete loss of mobility. In fact, 2 hours of treatment with H_2O_2 caused a strong decrease in movement (Figure 9a, mock), in contrast to the untreated animals. Interestingly, nanoalgosome treatment counteracted oxidative stress by increasing movement (one-way ANOVA mock vs nanoalgosome***, p=0.0009). This rescue was similar to one obtained with a positive control, N-AcetylCysteine (NAC) (nanoalgosome vs NAC ns, p=0.5252), a widely used antioxidant agent[54]. *C. elegans* copes with changes in ROS levels by expressing detoxifying genes, such as glutathione S-transferase *gst-4*[55]. To determine whether nanoalgosomes could also directly affect detoxification gene expression, we used a transgenic strain expressing GFP under the control of the *gst-4* promoter[56]. After chronic treatment with nanoalgosomes, we observed a significant decrease in *gst-4* expression levels, suggesting that nanoalgosomes can modulate detoxification gene expression (Figure 9b and Supporting Figure 7). Moreover, antioxidant molecules are capable of counteracting aging and motility decline[57]. In fact, the animal movement is influenced by aging and starting from three days from hatching (young adult stage) it slowly declines[58]. Therefore, we decided to assess nanoalgosome antioxidant effects by performing an acute treatment at very low concentration (10 µg/mL for 16 h), and we analyzed the locomotion of young adult animals (right after the treatment) and older animals (10 days from hatching, 7 days after treatment). As expected, we observed a physiological decline in locomotion between young and old animals (*t*-test mock young vs mock old*, p=0.0199) (Figure 9c). Interestingly, nanoalgosomes prevented aging effects by preserving the movement capability in older animals and keeping it similar to the one observed in younger animals (*t*-test mock old vs nanoalgosome old*, p<0.0362; nanoalgosome young vs nanoalgosome old ns, p=0.2037). Taken together, our results indicate that microalgal-derived EVs are bioactive with a clear antioxidant effect both *in vitro* and *in vivo*, supporting their potential role in counteracting aging at molecular and functional level, having the potential to be used as natural and innovative antioxidant effectors.

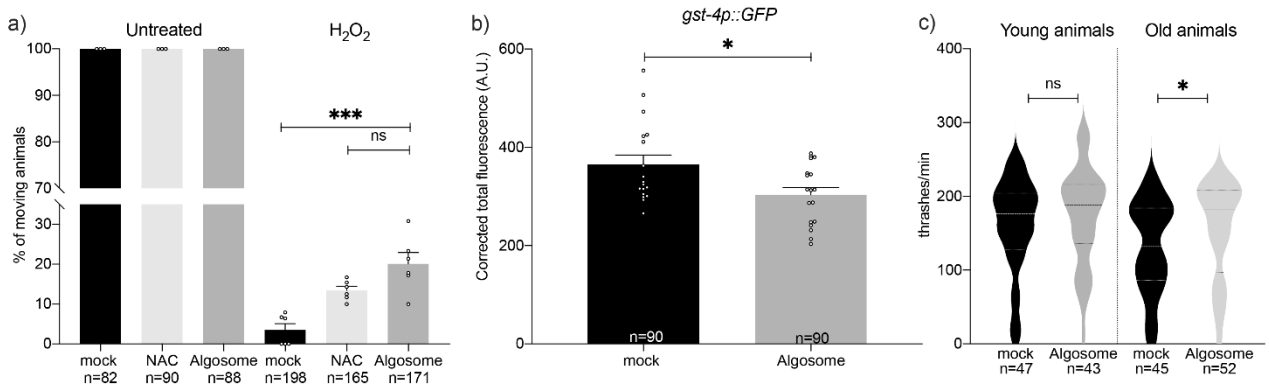

Figure 9. **Antioxidant and antiaging activity *in vivo* of nanoalgosomes in *C. elegans***. a) *In vivo* response to exogenous H_2O_2 stress. Animals have been treated with mock, NAC (2mM) and nanoalgosome (20 µg/mL). Animal movement was assessed right after acute exposure with water (untreated) or H_2O_2 5mM. Bars represent the mean and dots are replicates; error bar is the SEM. n is the number of animals analyzed. H_2O_2 mock vs H_2O_2 nanoalgosome***, p=0.0009; H_2O_2 nanoalgosome vs H_2O_2 NAC ns, p=0.5252. **b)** Quantification of the fluorescence in *gst-4p*::GFP expressing animals after chronic treatment with mock or nanoalgosomes (20 µg/mL). Each dot represents the total fluorescence in a picture corrected for the background. Bars represent the mean; error bar is the SEM. n is the total number of animals analyzed. *t*-test: mock vs nanoalgosome *p=0.0435. **c)** Thrashing assay on young and old animals after acute treatments with mock and nanoalgosomes (10 µg/mL). Violin plots show the distribution of thrashes performed by the animals in a minute. Bold dashed lines in the center correspond to the medians, while upper and lower dashed lines correspond to the quartiles. n is the number of animals analyzed. *t*-test: mock vs nanoalgosome treatment of young animals ns p=0.3387; mock vs nanoalgosome treatment of old animals * p<0.0362.

Anti-inflammatory activity of nanoalgosomes

The bioactivity of nanoalgosomes was investigated also in immune-responsive macrophage cells. Lipopolysaccharide (LPS) treatment of THP-1 cells induces the release of interleukin-6 (IL-6), which is a marker of inflammation. Initially, we checked the viability of THP-1 cells treated with different concentrations of nanoalgosomes for up to 72 hours, confirming that nanoalgosomes (up to 2 µg/mL) do not induce any cell toxicity (Supporting Figure 8). Subsequently, THP-1 cells were pre-treated with 0.5 µg/mL of nanoalgosomes for 4 hours and afterwards exposed to LPS-induced inflammation for 20 hours. We then monitored IL-6 induction in these samples using qRT-PCR and ELISA tests. The results in Figure 10 show no significant differences in IL-6 induction following 24 hours of nanoalgosome treatment compared to untreated cells; this result is in line with the *in vivo* data, previously shown, and is indicative of the immune-compatibility of nanoalgosomes. Further, figure 10 shows that the levels of IL-6 (a) mRNA and (b) protein were significantly lower compared to the condition without pre-incubation with nanoalgosomes. Indeed, nanoalgosomes significantly reduced IL-6 induction in LPS-treated THP-1 cells, leading to a 4.5-fold reduction in mRNA level and

a 7-fold reduction in IL-6 production, and indicating their anti-inflammatory activity *in vitro* (Figure 10).

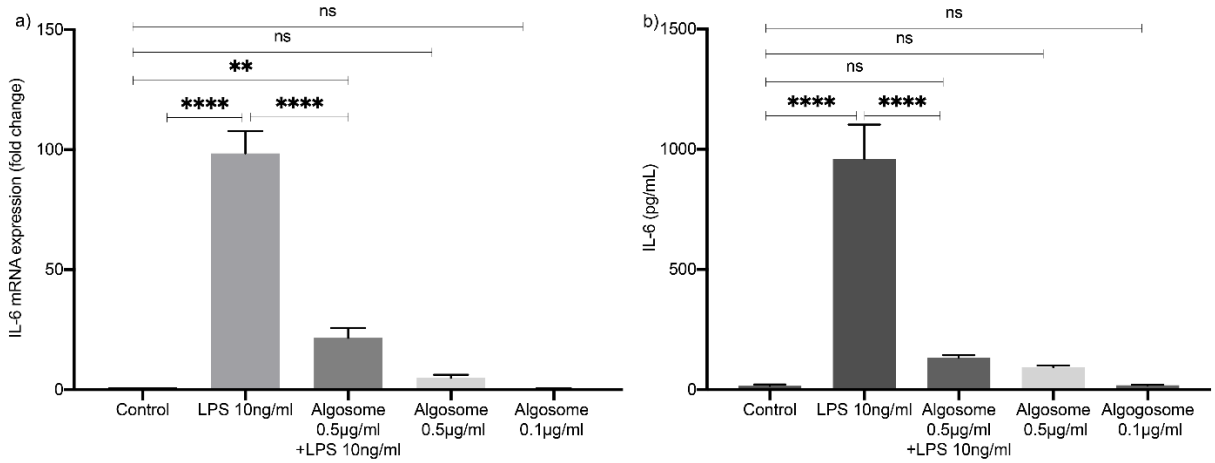

Figure 10. Anti-inflammatory effect of nanoalgosomes in immune-responsive cells. **a)** Real-time PCR quantification of mRNA for IL-6 relative levels after exposure with LPS (10 ng/mL) and nanoalgosomes (0.5 µg/mL) for 24h, in TPH-1 cells. **b)** Elisa results of IL-6 induction after exposure with LPS (10 ng/mL) and nanoalgosomes (0.5 µg/mL) for 24h, in TPH-1 cells. Two-way ANOVA statistical test was used to assess the statistical significance of the differences: Control vs LPS (10 ng/mL), LPS (10 ng/mL) vs Algosomes (0.5 µg/mL) + LPS (10 ng/mL), **p<0.01,****p<0.0001, ns=not significant. Representative results of three independent biological replicates.

In summary, this study demonstrates that nanoalgosomes are a new type of EVs endowed with unparalleled biocompatibility and unique tropism and bioactivities, including attributes making them suitable as innate antioxidant and anti-inflammatory effectors. Indeed, nanoalgosomes reduced the levels of reactive oxygen species and prevented oxidative stress in both tumoral and normal cell lines and in whole organisms, suggesting that they are enriched with antioxidant compounds. In addition, nanoalgosomes are immune-tolerated and exhibit an anti-inflammatory activity *in vitro.* Furthermore, they come with the capacity to be produced at mass scale, with a renewable and sustainable bioprocess from an edible source. This places this technology in an ideal situation to tap into the enormous and still underexploited potential of EVs as novel biological therapeutics, and eventually for further bioengineering to act as delivery vehicles for therapeutic agents.

.

METHODS

Resource availability

Further information and requests for resources and reagents should be directed to and will be fulfilled by the lead contact, Antonella Bongiovanni (antonella.bongiovanni@cnr.it).

Microalgae cultivation and nanoalgosome separation from microalgae-conditioned media

A stock culture of the marine chlorophyte *T. chuii* CCAP 66/21b was grown and nanoalgosome purification performed as previously described[15]. Briefly, after 30 days, 6 liters of microalgae cultures were clarified by microfiltration using a 450 nm hollow fiber cartridge housed in the KrosFlo® KR2i TFF System. Feed flow and transmembrane pressure (TMP) were kept constant at 750 mL/min and 0.05 bar, respectively. The 450 nm permeate (<450 nm sized particles) was subjected to a second microfiltration step using a 200 nm hollow fiber membrane at a 750 mL/min feed flow and 0.05 bar TMP. The resulting permeate (<200 nm sized particles) was ultrafiltrated by means of a 500 kDa MWCO hollow fiber membrane with a feed flow of 750 mL/min and 0.05 bar TMP, and concentrated to a final volume of 150 mL. Samples were concentrated and diafiltered seven times with PBS without calcium and magnesium (Sigma-Aldrich), using a smaller 500 kDa cutoff TFF filter module with a feed flow of 75 mL/min and 0.25 bar TMP, to a final volume of approximately 5 mL. Nanoalgosome protein content was measured using the Micro BCA Protein Assay Kit (Thermo Fisher Scientific), and nanoparticle size distribution and concentration were obtained using a NanoSight NS300 (Malvern Panalytical, UK)[15].

Nanoalgosome characterization

Nanoalgosomes are characterized as previously described in Adamo G. et al., 2021, and the relative methods are briefly reported in supporting methods[15].

Nanoalgosome staining

Nanoalgosomes were labeled with lipophilic dyes: Di-8-ANEPPS (Sigma-Aldrich) for endocytosis inhibition study and *in vivo* studies in *C. elegans*; PKH26 (Sigma-Aldrich) for intracellular trafficking studies; DiR (Sigma-Aldrich) for *in vivo* studies in mice.

Di-8-ANEPPS-, PKH-26- and DiR-nanoalgosome staining were performed as described[15, 24].

Briefly, for *in vivo* studies in mice, DiR-nanolgosome labeling was carried out by 30 minutes of incubation at room temperature with 3.5 µM of DiR diluted in PBS without calcium and magnesium. The same amount of DiR diluted in PBS was used as negative control of free dye. Next, both samples were analyzed by nanoparticle tracking analysis, to check nanoparticle size and distribution, following the removal of free dye by ultracentrifugation (118,000xg for 70 min at 4°C, twice)[15].The presence of DiR-fluorescence in nanoalgosome-labeled samples was verified by Odyssey scanner IR-measurements (Supporting Figure 2).

Cell lines

The following cell lines were used for the gene expression, bioactivity, and intracellular trafficking analyses: (i) 1–7 HB2, a normal mammary epithelial and (ii) MDA-MB 231, an epithelial human breast cancer and (iii) THP-1 human monocytic leukemia cell lines. All cells were maintained at 37°C in a humidified atmosphere (5% CO2)[15,24].

The THP-1 cell line (ECACC 88081201) was maintained in culture with RPMI 1640 medium (Gibco Life Technologies, Monza, Italy) supplemented with heat inactivated 10% Fetal Bovine Serum (FBS, Gibco Life Technologies, Monza, Italy) and 1% antibiotic (penicillin 5,000 U/mL, Streptomycin sulfate 5,000 µg/mL, Gibco Life Technologies, Monza, Italy). Cells were differentiated into macrophages by 72h incubation with 200 nM phorbol 12-myristate 13-acetate (PMA)[59].

C. elegans maintenance and strains

Nematodes have been grown and handled following standard procedures under uncrowded conditions on nematode growth medium (NGM) agar plates seeded with *Escherichia coli* strain OP50 [60]. Strains used in this work have been provided by the *Caenorhabditis* Genetics Center (CGC): wild-type strain N2 (Bristol variety); EG1285 *oxIs12* X *[unc-47p::GFP; lin-15(+)]*(expression of the Green Fluorescent Protein, GFP, in GABA neurons); VC2405 *chc-1(ok2369)* III/*hT2 [bli-4(e937) let-?(q782) qIs48]* (I;III) (knockout mutant of *chc-1)*; RT1315 *unc-119(ed3)* III, *pwIs503 [vha-6p::mans::GFP + Cbr-unc-119(+)]* (expression of an intestine-specific GFP marker for the Golgi apparatus); RT476 *unc-119(ed3) III; pwIs170 [vha6p::GFP::rab-7 + Cbr-unc-119(+)]* (expression of an intestine-specific GFP marker for late endosomes); CL2166 *dvIs19* III [(pAF15) *gst-4p::GFP::NLS*] (expression of an oxidative stress-responsive GFP). Strain QH3803 *vdEx263 [mec-4p::mCherry; odr-1p::dsRed]* expressing mCherry in mechanosensory neurons was kindly provided by M.A. Hilliard (QBI, University of Queensland, Australia)[61]. BY250 *vtIs7 [dat-1p::GFP]* expressing GFP in dopaminergic neurons was kindly provided by M. Aschner (Albert Einstein College of Medicine, NY, USA)[62].

Biocompatibility *in vivo* assays in *C. elegans*

For the assessment of nanoalgosome toxicity *in vivo*, *C. elegans* synchronized animals have been treated with PBS as mock or nanoalgosomes at different concentrations (1, 20, 64 and 128 µg/mL), through *in liquido* culturing in 96-multiwell plates for 72 h[24]. Synchronized eggs were obtained by bleaching and resuspended in M9 buffer (3 g KH_2PO_4; 6 g Na_2HPO_4; 5 g NaCl; 1 M $MgSO_4$; H_2O to 1 L) with 2x antibiotic/antimycotic solution (Sigma-Aldrich, A5955), 5 ng/mL cholesterol and OP50 bacteria. 60 µL of this mix containing approximately a total of 30 eggs were aliquoted in each well. After 72 h the number of living animals and of animals reaching the adult stage was quantified per each replicate, with a minimum number of replicates corresponding to three.

For the growth assay, synchronized animals have been treated *in solido* on NGM plates seeded with heat-killed (45 min at 65°C) OP50 bacteria and nanoalgosomes (20 µg/mL final concentration), or PBS buffer as mock. The dilutions were performed considering a final volume of NGM in the plate of 4 mL[24]. ~20 adults per plate in triplicate were let lay eggs for 2 h to obtain synchronized eggs. Animal

stage was quantified in each plate every 24 h for 4 days, and the percentage of animals at each stage was calculated on the total number of animals present on the plate.

For the lifespan assay, synchronized animals have been treated *in solido,* as described above, with nanoalgosome at a final concentration of 20 µg/mL and PBS as mock. Viability was scored each 3 days and animals were transferred every 3 days in fresh plates with nanoalgosome or mock, respectively. To test the nanoalgosome effect on brood size and embryonic vitality, 20 animals were treated *in solido,* as described above, until L4 larval stage and then transferred to new plates without any treatment. Then, every 24 h animals were moved to new plates without any treatment for all the fertile period of the animals (4 days) and the number of laid and hatched eggs counted every day, treatments were performed in triplicate[63]. To assess a putative nanoalgosome neurotoxicity, animals expressing fluorescent protein in GABAergic, mechanosensory and dopaminergic neurons were treated *in liquido* in triplicate*,* as described above. After 72 h of treatment animals were immobilized with 0.01% tetramisole hydrochloride (Sigma-Aldrich, T1512) on 4% agar pads for microscopy analysis and the morphology and the total number of visible fluorescent neurons was quantified in each animal[61,64, 65]. Confocal images were collected with a Leica TCS SP8 AOBS microscope using a 20x objective.

DNA damage *in vitro* and *in vivo*

Gene expression analyses *in vitro.* Quantitative analysis of mRNA expression were performed in 1-7 HB2 cells. Specifically, $5x10^3$ cells were treated with 2 µg/mL of nanoalgosomes for 24h for genotoxicity study, in which *ATR, CHECK1, RAD51* genes were chosen to assess the expression of DNA damage-related genes. Treatments were performed in triplicate.

RNA extraction and first-strand cDNA synthesis. Total RNA was extracted from control and treated cells using TRIzol Reagent (Invitrogen), following the manufacturer's instructions, and then stored at −80°C until used. Purified RNA was treated with DNase I, Amplification Grade (Sigma-Aldrich) at 37°C for 30 min to remove any residual genomic DNA contamination, and DNase I was inactivated by adding 50 mM EDTA. First-strand cDNA was synthesized from DNase I-treated RNA samples using the High-Capacity cDNA Reverse Transcription Kit (Thermo Fischer Scientific) following the manufacturer's instructions. The cDNA mixture was tested by PCR using GAPDH and ACTB primers and diluted 1:5 before use in Real-Time qPCR experiments.

Gene expression by real-time qPCR. The qPCRs were performed using the BIO-RAD CFX96 system with BlasTaq 2X qPCR MasterMix (Applied Biological Materials) as detection chemistry[66]. *ACTB* and *GAPDH* genes were selected as control genes based on their expression stability in all tested conditions. A normalization factor was calculated based on geometric averaging of *ACTB*, and *GAPDH* expression and was used to quantify target gene mRNA levels. Serial dilutions of pooled cDNAs from both control and treated samples were prepared to determine the PCR efficiency of the target and reference genes (data not shown), with amplification efficiency ranging from 1.9 to 2.1. The primer sequences used are listed in Supporting table 3. The qPCRs were conducted according

to the manufacturer's recommendations, and each reaction was repeated in triplicate. Amplification conditions were: initial denaturation at 95°C for 3 min and 40 cycles of 95°C for 15 s and 60°C for 60 s, followed by a melting curve from 60°C to 95°C. Amplicons were detected by agarose gel analysis after each PCR to confirm the amplification of the specific gene product (data not shown).

Genotoxicity assay in *C. elegans*. For germline apoptosis quantification, animals were treated *in liquido* as described above, with nanoalgosome at a final concentration of 20 µg/mL, PBS as mock and doxorubicin 2.4 µM as positive control. After 72 h of treatment animals were stained by incubation with 33 µM SYTO™12 (Invitrogen, S7574) for 1 h and 30 min at room temperature in the dark. Animals were cleaned by crawling in fresh plates for 30. For microscopy analysis animals were immobilized as above and the quantification of apoptosis after treatment was calculated as the average number of apoptotic corpses per gonadal arm[42].

Flow cytometry-based basophil activation test

Heparinized peripheral blood was obtained from 3 volunteers. The potential allergenic activity of nanoalgosomes was studied by basophil activation in whole blood samples using flow cytometry to detect the combination of CCR3 and CD63 markers by means of the Flow CAST Basophil Activation Test (Buhlmann Laboratories AG, Switzerland). Blood aliquots (100 µl) were incubated with nanoalgosome dilutions (0.025 - 0.5 - 1 - 2 µg/mL, according to the BCA analysis) in RPMI for 15 minutes at 37°C. PBS and anti-Fc Epsilon RI were used as negative and positive controls, respectively. Results were analyzed using WinMDI 2.8 software (Scripps Research Institute, Jupiter). Basophil activation was reported when more than 5% of activated cells were detected (according to the manufacturer's instructions). The study was approved by the local Ethics Committee (Comitato Etico Palermo 1, 24 February 2021, resolution n. 02/2021).

In vivo experiments in mice

All animal experiments were performed on wild type BALB/c and athymic nude mice, male and female, which were purchased from Janvier Labs (France) at 5 weeks of age. Animals were used in accordance with Cellvax approved standard operation procedures, in which food and water were provided *ad libitum*. Mice were housed in specific pathogen-free conditions in compliance with the Federation of European Laboratory Animal Science Association (FELASA) guidelines. Housing conditions entailed a 12:12 light:dark cycle, room temperature at 20±2°C°, and 70% relative humidity. Mice were acclimatized for one week and were regularly handled by personnel for gentling and habituating to the procedures. On the day of the experiment, animals were randomly allocated into 3 different treatment groups. For the biodistribution study, groups consisted of 3 male and 3 female athymic nude mice (n_1=6), while for the biocompatibility study, groups contained 2 male and 2 female BALB/c mice (n_2=4). Each group received a different treatment, and sex was imposed as blocking factor for the statistical analysis. The results were presented as mean ± σ (n_1=6; n_2=4). Multiple comparisons between the groups were performed using GraphPad software.

Nanoalgosome biocompatibility study in mice. BALB/c mice (4 animals/group) were injected in the ocular vein (using 1mL insulin syringes with a 25G needle) with nanoalgosome formulations (**dose 1**: 10µg corresponding to $4x10^{10}$ nanoalgosomes/200 µL/mouse; **dose 2**: 50µg corresponding to $2x10^{11}$ nanoalgosomes/200 µL/mouse and **control**: v/v of free dye control /200 µL/mouse).
Animals were examined clinically daily. A thorough examination was done once a week and included: clinical signs, behavior, signs of suffering (cachexia, weakening, and difficulty of moving or feeding, etc.) and nanoalgosome toxicity (hunching, convulsions). Body weight was monitored once a week and a body weight curve were designed (Mean±SD). Acute reactions were observed after dose administrations. Mouse daily clinical status analyses were performed during nanoalgosome treatments. For toxicity and tolerance evaluation, a distress score was recorded and included in weekly reporting: parameter 1 (appearance), parameter 2 (application site appearance), parameter 3 (natural behavior), parameter 4 (knee swelling), parameter 5 (compound toxicity hunching & convulsion), parameter 6 (food and water intake).
Biochemical and hematological analysis. For each animal, 100µL of blood (in compliance with the National Centre for the Replacement, Refinement and Reduction of Animals in Research guidelines) was collected from the lateral tail vein at 3h, 6h, 24h, 48h. Animals were euthanized after the last sampling point with CO_2 (slow fill rate and organ harvesting performed after confirmation of death). Blood was collected and stored in K_2-EDTA BD-Microtainers (Thermo Fisher Scientific), centrifuged at 4°C, at 3000 g for 5 min and the obtained plasma (25µL) stored at −20 C. The blood parameters analyzed were hematocrit, lymphocyte count, creatinine, and BUN.
Nanoalgosome biodistribution in the mouse model. IVIS spectrum studies: The biodistribution of the fluorescently labeled nanoalgosomes was determined by *in vivo* near-infrared fluorescence imaging using an IVIS Spectrum scanner (IVIS Spectrum CT; PerkinElmer). Athymic nude mice (6 animals/group) were anesthetized with 5% isoflurane in 100% O_2 at 1L/min for induction, and anesthesia was maintained with 1.2 minimum alveolar concentration via face mask while mice were injected in the ocular vein (as above) with the DiR labeled formulations (listed above) and images were acquired at different post-injection time points (3, 6, 24, 48h). The IVIS Spectrum scanner was set to fluorescence imaging mode, time and an emission filter positioned at 650nm. The focus was kept stable using subject high of 1.5 cm whereas the temperature of the chamber was set at 37°C. Image analyses (set with a fixed count scales from 1′000 to 40′000 and acquired with a 0.2 s exposure time) were computed by first defining the regions of interest (ROI; a representative image with the ROIs are shown in figure 5), which were kept consistent across images, and then the sum of all counts for all pixels inside the ROI (Total Fluorescence Counts-TFqC; photons/second) was recorded.

Endocytosis inhibition study in cellular models

To study the specific endocytic mechanism involved during nanoalgosome uptake, 1-7 HB2 cells ($5x10^3$/wells) were seeded in a 96-well plate. After 24 h, cells were pre-incubated with

pharmacological/chemical inhibitors before nanoalgosome addition. Next, the dose- and time-dependent effect of each inhibitor on nanoalgosome cellular uptake was determined. In particular, cells were pre-incubated with the following inhibitors: dynasore (a clathrin-mediated endocytosis inhibitor) at 10, 30, 60, 80 µM; EIPA (5-[N-ethyl-N-isopropyl] amiloride, a pinocytosis/macropinocytosis inhibitor) at 1, 5, 10, 25 µM; nystatin (a caveola/lipid raft-mediated endocytosis inhibitor) at 5, 10, 25, 50 µM. Cells were pre-incubated with dynasore and EIPA for 60 min at 37°C and washed prior to nanoalgosome addition. Cells were pre-incubated with nystatin for 30 min at 37°C. Next, 10 µg/mL Di-8-ANEPPS-labeled nanoalgosomes were added to cells in the presence of these blocking agents, and were subsequently kept at 37°C up to 3h. The cells treated with nanoalgosomes without inhibitor treatment were used as negative control, while positive control cells were incubated at 4°C to inhibit all energy-dependent mechanisms. Intracellular fluorescence was monitored after 2 and 3 h of nanoalgosome incubation by spectrofluorimetric analysis using a microplate reader (Glomax, Promega). As vehicle-control, cells were cultured in the presence of methanol. A cell viability assay was performed after each treatment (Supporting Figure 4), and treatments were performed in triplicate.

Nanoalgosome intracellular localization *in vitro*

The MDA-MB 231 cell line was grown at a density of $5x10^3$ cells/well in 12-well plates containing sterile coverslips in complete medium for 24 h. Cells were incubated with 2 µg of PKH-26-labeled nanoalgosomes at 37°C for 24 h. Cells were then washed twice with PBS, fixed with 3.7% paraformaldehyde for 15 min, and washed twice with PBS. Afterwards, cells were permeabilized with 0.1% Triton 100-X in PBS with Ca^{++} and Mg^{++} for 10 m at room temperature. Next, cells were incubated with 1% bovine serum albumin (Sigma-Aldrich) in PBS for 30 m at room temperature to block unspecific binding of the antibodies. Cells were incubated in a primary antibody (CD63 for the endosomal system, clone MX-49.129.5, VWR, anti-LAMP1 for lysosomes, clone 1D4B, Sigma-Aldrich, and anti-calnexin for ER, clone NB100-1965, Novus Biologicals) diluted in blocking solution for 1h at 37°C. Cells were then incubated with a secondary antibody (AlexaFluor-488; Thermo Fischer Scientific) and diluted in blocking solution (1:50) for 2 h at room temperature. Coverslips were mounted with a drop of Vectashield Mounting Medium with DAPI (Sigma-Aldrich). Nanoalgosome intracellular localization was monitored by confocal laser scanning microscopy (Olympus FV10i, 1 µm thickness optical section was taken on a total of about 15 sections for each sample) and fluorescence microscopy analysis (Nikon Eclipse 80i).

In vivo subcellular localization and internalization mechanism in *C. elegans*

For subcellular localization and to identify the internalization mechanism, transgenic or mutant animals were treated *in solido.* ~20 synchronized L4 larvae were transferred on freshly prepared NGM plates seeded with heat-killed OP50 bacteria and Di-8-Anepps labelled nanoalgosome (20 µg/mL final concentration) as described in Picciotto et al., 2022. After 24 h of treatment in the dark, young adult animals were transferred to clean NGM plates with OP50 bacteria to let the animals

crawl for 1 h to remove the excess of dye. Animals were immobilized as above and confocal images were collected with a Leica TCS SP8 AOBS microscope using a 40x objective.

In vitro bioactivity assay in cellular models

Intracellular ROS levels of living cells were determined using 2′, 7′- dichlorofluorescein diacetate (DCF-DA; Sigma-Aldrich). DCF-DA is oxidized to fluorescent DCF (2′, 7′- dichlorofluorescein) in the presence of ROS, which can be readily detected by a spectrofluorometer. We performed an antioxidant assay on tumoral (MDA-MB 231) and normal (HB2 1-7) cell lines. Briefly, $4x10^3$ cells were cultured in 96-well microplates for 24 h. Cells were then incubated with different concentrations of nanoalgosomes (0.5, 1 and 2 µg/mL) for 24 h. The medium was removed and cells were exposed to PBS containing 40 µM of DCF-DA and kept in a humidified atmosphere (with 5% CO_2 at 37°C) for 1 h. Next, cells were treated with/without the oxidative agent H_2O_2 (250 µM for 3 h) or TBH (250 µM for 1 h) (tert-butyl hydroperoxide solution, Sigma-Aldrich) in the absence/presence of nanoalgosomes. Untreated cells were used as a control to set the percentage of basal intracellular ROS. After extensive washing steps, fluorescence intensity was quantified using a fluorescence plate reader at an excitation of 485 nm and an emission of 538 nm (GloMax® Discover Microplate Reader, Promega).

The relative percentage of intracellular ROS was normalized with respect to untreated cells (control). A cell viability assay was performed after each treatment (see supporting methods). For gene expression analysis related to antioxidant activity of nanoalgosomes, quantitative analysis of mRNA expression was performed on 1-7 HB2 cells (as described above) and included *CAT*, *GPX*, *GSR*, *AKR, FTH*, *ALOX*, *and NOS*. $5x10^3$ cells were incubated with nanoalgosomes (2 µg/mL) for 24 h, then, the medium was removed and cells were exposed to oxidative stress (250 µM of H_2O_2, Sigma-Aldrich, Germany) for 3 h. Untreated cells were used as negative control.

In vivo bioactivity assays in *C. elegans*

For the assessment of exogenous H_2O_2 stress response, animals have been treated *in liquido* as described above for 72 h with nanoalgosome at 20 µg/mL final concentration, PBS as mock and N-AcetylCysteine (NAC) (Sigma-Aldrich, A7250) 2mM as positive control. After treatment, animals were exposed to H_2O_2 5mM and water as control for 2 h, then transferred to fresh NGM plates with OP50 bacteria and the number of moving animals on the total number of animals on the plate was scored.

gst-4p::GFP expression was quantified after 72 h of treatment *in liquido,* as described above. 5 animals on each slide were immobilized as above, this time using 100 mM NaN_3 (Sigma-Aldrich, S8032) to allow the lineup of animals. Epi-fluorescence images were collected with a Leica TCS SP8 AOBS inverted microscope, using a 10x objective and FITC filter. Fluorescence quantification was performed using ImageJ, and the Corrected Total Fluorescence (CTF) was calculated for each image using this formula: (integrated density of the area containing the animals) – [(area containing

the animals) x (mean fluorescence of background)][63]. Representative pictures in supporting figure 7 were pseudo-colored using Image J.

The anti-aging effect of nanoalgosome on animal movement was assessed through the thrashing assay on young (3 days from hatching) and old (10 days from hatching). Animals at young adult stage have been treated for 16 h *in liquido* with nanoalgosome at a final concentration of 10 µg/mL and PBS used as mock. After treatment animals were transferred to fresh NGM plates and young animals were immediately analyzed, while old animals were transferred every 2 days in fresh plates until day 10 from hatching. For video recording animals were transferred in 7µL of M9 buffer, left 5 minutes to acclimate and then recorded for 30 seconds. The measurement of thrashing was done counting every change of direction respect to the longitudinal axis of the body[67]. Treatments were performed in triplicate.

Anti-inflammatory Activity Assay

1×10^6 cells/mL THP-1 cells were seeded in 24-well in complete medium. After 24 hours, cells were pre-incubated with nanoalgosomes (0.5 µg/mL) for 4 h. After 4 h of pre-incubation, cells were subjected to an inflammatory stimulus, by adding lipopolysaccharide (10 ng/mL LPS from E. coli O55: B5, Sigma-Aldrich) for 20h. Cells stimulated with LPS for 20h (without pre-incubation with nanoalgosomes) represented the positive controls. In addition, cells were incubated with different amounts of nanoalgosomes (0.5 and 0.1 µg/mL) for 24h. Untreated cells are used as negative controls. Experiments were performed in triplicate.

Cytokine expression - Real Time PCR analysis

Total RNA was extracted using the QIAzol Lysis Reagent protocol (Qiagen) according to the manufacturer's instructions. The cDNA synthesis was performed using the QuantiTect Reverse Transcription Kit (Qiagen) with 2.5 µg of total RNA. The cDNA was diluted up to 100 µl, and Real Time analyses were performed with an Applied Biosystems StepOnePlusTM Real Time PCR System and Sybr Green technology. Each sample contained 1-100 ng of cDNA in PowerTrack SYBR Green Master Mix (Applied Biosystems, Thermo Fisher Scientific) and 200 nM of specific Quantitect primer assay (Qiagen) in a final volume of 20 µl. The primer sequences used for human cytokines were hIL-6 (Interleukin 6, NM_000600) and the PCR conditions were 95°C for 20 seconds, followed by 40 cycles of two-step PCR denaturation at 95°C for 15 seconds and annealing/extension at 60°C for 30 seconds.

Inflammatory Cytokine Test

IL-6 levels in supernatants were determined using commercially available human IL-6 ELISA kits according to the manufacturer's protocol (Human IL-6 ELISA Kit, Invitrogen). Medium supernatant and standards were added to the wells and incubated at room temperature for 1h on a horizontal shaker set at 700 rpm ± 100 rpm. Then, the plates were washed and anti-IL-6 conjugate was add into all the wells incubated for 1 h at room temperature on a horizontal shaker set at 700 rpm ± 100 rpm.. The plates were washed again and Chromogenic TMB was add to each well. The substrate

solution begins to turn blue. After incubation for 15 minutes at room temperature on a horizontal shaker set at 700 rpm ± 100 rpm in the dark, stop solution was added and the optical densities were read at 450 nm wavelength. The results of IL-6 were expressed as concentrations as pg/mL, using standard calibration curve of IL-6. The data were expressed as mean±standard deviation.

Statistics and reproducibility

Statistical analyses were performed with GraphPad Prism software. The experimental replicates and statistical analyses used for each experiment are described in the figure legends.

References

1. Yáñez-Mó, M. *et al.* Biological properties of extracellular vesicles and their physiological functions. *J Extracell Vesicles* **4**, 10.3402/jev.v4.27066 (2015).
2. Vardi (Schatz D, Vardi A. Extracellular vesicles - new players in cell-cell communication in aquatic environments. Curr Opin Microbiol. 2018;43:148–54.)
3. Li, M. *et al.* Extracellular vesicles as bioactive nanotherapeutics: An emerging paradigm for regenerative medicine. *Theranostics* **12**, 4879–4903 (2022).
4. Saleh, A. F. *et al.* Extracellular vesicles induce minimal hepatotoxicity and immunogenicity. *Nanoscale* **11**, 6990–7001 (2019).
5. Herrmann, I. K., Wood, M. J. A. & Fuhrmann, G. Extracellular vesicles as a next-generation drug delivery platform. *Nat Nanotechnol* **16**, 748–759 (2021).
6. Elsharkasy et al. Extracellular vesicles as drug delivery systems: Why and how? Adv. Drug. Deliv. Rev., 2020.
7. Witwer and Wolfram Extracellular vesicles versus synthetic nanoparticles for drug delivery. Nature Reviews Materials 2022
8. . Sun, Y. *et al.* Mesenchymal stem cells-derived exosomes for drug delivery. *Stem Cell Res Ther* **12**, 561 (2021).
9. Warnecke, A. *et al.* First-in-human intracochlear application of human stromal cell-derived extracellular vesicles. *J Extracell Vesicles* **10**, e12094 (2021).
10. Paganini et al. Scalable production and isolation of EVs: Available sources and lessons from current industrial bioprocesses. Biotechnol. J., 2019.
11. Zarovni, N. *et al.* Standardization and Commercialization of Extracellular Vesicles. (2021) doi:10.1039/9781839164552-00303.
12. Kameli, N., Dragojlovic-Kerkache, A., Savelkoul, P. & Stassen, F. R. Plant-Derived Extracellular Vesicles: Current Findings, Challenges, and Future Applications. *Membranes* **11**, 411 (2021).
13. Sanwlani, R., Fonseka, P., Chitti, S. V. & Mathivanan, S. Milk-Derived Extracellular Vesicles in Inter-Organism, Cross-Species Communication and Drug Delivery. *Proteomes* **8**, 11 (2020).
14. Gerritzen, M. J. H., Salverda, M. L. M., Martens, D. E., Wijffels, R. H. & Stork, M. Spontaneously released Neisseria meningitidis outer membrane vesicles as vaccine platform: production and purification. *Vaccine* **37**, 6978–6986 (2019).
15. Adamo, G. *et al.* Nanoalgosomes: Introducing extracellular vesicles produced by microalgae. *Journal of Extracellular Vesicles* **10**, e12081 (2021).
16. Picciotto, S. *et al.* Isolation of extracellular vesicles from microalgae: towards the production of sustainable and natural nanocarriers of bioactive compounds. *Biomater. Sci.* **9**, 2917–2930 (2021).
17. Paterna, A. *et al.* Isolation of Extracellular Vesicles From Microalgae: A Renewable and Scalable Bioprocess. *Front Bioeng Biotechnol* **10**, 836747 (2022).
18. Parkes, R., Barone, M. E., Herbert, H., Gillespie, E. & Touzet, N. Antioxidant Activity and Carotenoid Content Responses of Three Haematococcus sp. (Chlorophyta) Strains Exposed to Multiple Stressors. *Appl Biochem Biotechnol* **194**, 4492–4510 (2022).
19. Archer, L. *et al.* Antioxidant Bioprospecting in Microalgae: Characterisation of the Potential of Two Marine Heterokonts from Irish Waters. *Appl Biochem Biotechnol* **193**, 981–997 (2021).
20. Tan, J. S. *et al.* A review on microalgae cultivation and harvesting, and their biomass extraction processing using ionic liquids. *Bioengineered* **11**, 116–129 (2020).
21. Sansone, C. *et al.* The green microalga *Tetraselmis suecica* reduces oxidative stress and induces repairing mechanisms in human cells. *Scientific Reports* **7**, (2017).
22. Hyung, J.-H., Kim, E.-J., Moon, S.-J., Kang, N. S. & Park, J. Tetraselmis jejuensis sp. nov. (Chlorodendrophyceae), a Euryhaline Microalga Found in Supralittoral Tide Pools at Jeju Island, Korea. *Plants* **10**, 1289 (2021).
23. Coulombier, N., Jauffrais, T. & Lebouvier, N. Antioxidant Compounds from Microalgae: A Review. *Marine Drugs* **19**, 549 (2021).
24. Picciotto, S. *et al.* Extracellular Vesicles From Microalgae: Uptake Studies in Human Cells and Caenorhabditis elegans. *Front Bioeng Biotechnol* **10**, 830189 (2022).

25. Yao, Y., Zhang, T. & Tang, M. A critical review of advances in reproductive toxicity of common nanomaterials to Caenorhabditis elegans and influencing factors. *Environmental Pollution* **306**, 119270 (2022).
26. Hunt, P. R. The C. elegans model in toxicity testing. *Journal of Applied Toxicology* **37**, 50–59 (2017).
27. Choi, H. *et al.* Biodistribution of Exosomes and Engineering Strategies for Targeted Delivery of Therapeutic Exosomes. *Tissue Eng Regen Med* **18**, 499–511 (2021).
28. Escudé Martinez de Castilla, P. *et al.* Extracellular vesicles as a drug delivery system: A systematic review of preclinical studies. *Adv Drug Deliv Rev* **175**, 113801 (2021).
29. Driedonks, T. *et al.* Pharmacokinetics and biodistribution of extracellular vesicles administered intravenously and intranasally to *Macaca nemestrina*. *J of Extracellular Bio* **1**, (2022).
30. Gupta, D., Zickler, A. M. & El Andaloussi, S. Dosing extracellular vesicles. *Advanced Drug Delivery Reviews* **178**, 113961 (2021).
31. Tieu, A. *et al.* An Analysis of Mesenchymal Stem Cell-Derived Extracellular Vesicles for Preclinical Use. *ACS Nano* **14**, 9728–9743 (2020).
32. Somiya, M., Yoshioka, Y. & Ochiya, T. Biocompatibility of highly purified bovine milk-derived extracellular vesicles. *Journal of Extracellular Vesicles* **7**, 1440132 (2018).
33. Urzì, O., Raimondo, S. & Alessandro, R. Extracellular Vesicles from Plants: Current Knowledge and Open Questions. *International Journal of Molecular Sciences* **22**, 5366 (2021).
34. Maréchal, A. & Zou, L. DNA Damage Sensing by the ATM and ATR Kinases. *Cold Spring Harb Perspect Biol* **5**, a012716 (2013).
35. Rx, H. & Pk, Z. DNA damage response signaling pathways and targets for radiotherapy sensitization in cancer. *Signal transduction and targeted therapy* **5**, (2020).
36. Zhou, B.-B. S. & Elledge, S. J. The DNA damage response: putting checkpoints in perspective. *Nature* **408**, 433–439 (2000).
37. Nam, E. A. & Cortez, D. ATR signaling: more than meeting at the fork. *Biochem J* **436**, 527–536 (2011).
38. Liu, Q. *et al.* Chk1 is an essential kinase that is regulated by Atr and required for the G2/M DNA damage checkpoint. *Genes Dev* **14**, 1448–1459 (2000).
39. Gumienny, T. L., Lambie, E., Hartwieg, E., Horvitz, H. R. & Hengartner, M. O. Genetic control of programmed cell death in the Caenorhabditis elegans hermaphrodite germline. *Development* **126**, 1011–1022 (1999).
40. Papaluca, A. & Ramotar, D. A novel approach using C. elegans DNA damage-induced apoptosis to characterize the dynamics of uptake transporters for therapeutic drug discoveries. *Sci Rep* **6**, 36026 (2016).
41. Silva, N., Adamo, A., Santonicola, P., Martinez-Perez, E. & La Volpe, A. Pro-crossover factors regulate damage-dependent apoptosis in the Caenorhabditis elegans germ line. *Cell Death Differ* **20**, 1209–1218 (2013).
42. Santonicola, P., Germoglio, M., d'Abbusco, D. S. & Adamo, A. Functional characterization of Caenorhabditis elegans cbs-2 gene during meiosis. *Sci Rep* **10**, 20913 (2020).
43. Lai, C. P. *et al.* Dynamic biodistribution of extracellular vesicles in vivo using a multimodal imaging reporter. *ACS Nano* **8**, 483–494 (2014).
44. Lázaro-Ibáñez, E. *et al.* Selection of Fluorescent, Bioluminescent, and Radioactive Tracers to Accurately Reflect Extracellular Vesicle Biodistribution in Vivo. *ACS Nano* **15**, 3212–3227 (2021).
45. Mulcahy, L. A., Pink, R. C. & Carter, D. R. F. Routes and mechanisms of extracellular vesicle uptake. *J Extracell Vesicles* **3**, (2014).
46. Macia, E. *et al.* Dynasore, a Cell-Permeable Inhibitor of Dynamin. *Developmental Cell* **10**, 839–850 (2006).
47. Banizs, A. B., Huang, T., Nakamoto, R. K., Shi, W. & He, J. Endocytosis Pathways of Endothelial Cell Derived Exosomes. *Mol Pharm* **15**, 5585–5590 (2018).
48. Tian, T. *et al.* Exosome uptake through clathrin-mediated endocytosis and macropinocytosis and mediating miR-21 delivery. *J Biol Chem* **289**, 22258–22267 (2014).
49. Delenclos, M. *et al.* Investigation of Endocytic Pathways for the Internalization of Exosome-Associated Oligomeric Alpha-Synuclein. *Front Neurosci* **11**, 172 (2017).

50. Eom, H.-J. & Choi, J. Clathrin-mediated endocytosis is involved in uptake and toxicity of silica nanoparticles in Caenohabditis elegans. *Chem Biol Interact* **311**, 108774 (2019).
51. Borowitzka, M. A. High-value products from microalgae—their development and commercialisation. *J Appl Phycol* **25**, 743–756 (2013).
52. Plaza, M., Herrero, M., Cifuentes, A. & Ibáñez, E. Innovative natural functional ingredients from microalgae. *J Agric Food Chem* **57**, 7159–7170 (2009).
53. Das, K. & Roychoudhury, A. Reactive oxygen species (ROS) and response of antioxidants as ROS-scavengers during environmental stress in plants. *Frontiers in Environmental Science* **2**, (2014).
54. Ezeriņa, D., Takano, Y., Hanaoka, K., Urano, Y. & Dick, T. P. N-Acetyl Cysteine Functions as a Fast-Acting Antioxidant by Triggering Intracellular H2S and Sulfane Sulfur Production. *Cell Chemical Biology* **25**, 447-459.e4 (2018).
55. Hu, Q., D'Amora, D. R., MacNeil, L. T., Walhout, A. J. M. & Kubiseski, T. J. The Caenorhabditis elegans Oxidative Stress Response Requires the NHR-49 Transcription Factor. *G3 Genes|Genomes|Genetics* **8**, 3857–3863 (2018).
56. Cd, L. & Cj, J. Reporter transgenes for study of oxidant stress in Caenorhabditis elegans. *Methods in enzymology* **353**, (2002).
57. Sugawara, T. & Sakamoto, K. Quercetin enhances motility in aged and heat-stressed Caenorhabditis elegans nematodes by modulating both HSF-1 activity, and insulin-like and p38-MAPK signalling. *PLoS One* **15**, e0238528 (2020).
58. Herndon, L. A., Wolkow, C. A., Driscoll, M. & Hall, D. H. Effects of Ageing on the Basic Biology and Anatomy of C. elegans. in *Ageing: Lessons from C. elegans* (eds. Olsen, A. & Gill, M. S.) 9–39 (Springer International Publishing, 2017). doi:10.1007/978-3-319-44703-2_2.
59. Longo, V. *et al.* In vitro exposure to 2,2',4,4'-tetrabromodiphenyl ether (PBDE-47) impairs innate inflammatory response. *Chemosphere* **219**, 845–854 (2019).
60. Brenner, S. THE GENETICS OF CAENORHABDITIS ELEGANS. *Genetics* **77**, 71–94 (1974).
61. Kirszenblat, L., Neumann, B., Coakley, S. & Hilliard, M. A. A dominant mutation in *mec-7/β-tubulin* affects axon development and regeneration in *Caenorhabditis elegans* neurons. *MBoC* **24**, 285–296 (2013).
62. González-Hunt, C. P. *et al.* Exposure to mitochondrial genotoxins and dopaminergic neurodegeneration in Caenorhabditis elegans. *PLoS One* **9**, e114459 (2014).
63. Romano, M. *et al.* Synthesis and Characterization of a Biocompatible Nanoplatform Based on Silica-Embedded SPIONs Functionalized with Polydopamine. *ACS Biomaterials Science & Engineering* **9**, (2022).
64. Hensel, N. *et al.* Impairment of the neurotrophic signaling hub B-Raf contributes to motoneuron degeneration in spinal muscular atrophy. *Proc. Natl. Acad. Sci. U.S.A.* **118**, e2007785118 (2021).
65. Illiano, P. *et al.* A Caenorhabditis elegans model to study dopamine transporter deficiency syndrome. *Eur J Neurosci* **45**, 207–214 (2017).
66. Vandesompele, J., Preter, K. D., Roy, N. V. & Paepe, A. D. Accurate normalization of real-time quantitative RT-PCR data by geometric averaging of multiple internal control genes.
67. Di Giorgio, M. L. *et al.* WDR79/TCAB1 plays a conserved role in the control of locomotion and ameliorates phenotypic defects in SMA models. *Neurobiol Dis* **105**, 42–50 (2017).

FUNDING

This work was supported by the VES4US and the BOW projects funded by the European Union's Horizon 2020 research and innovation programme, under grant agreements Nos 801338 and 952183.

ACKNOWLEDGEMENTS

The authors thank for *C. elegans* strains M.A. Hilliard (QBI, University of Queensland, Australia), M. Aschner (Albert Einstein College of Medicine, NY, USA), S. Martinelli (ISS, Rome, Italy) and CGC, which is funded by NIH Office of Research Infrastructure Programs (P40 OD010440).

AUTHOR CONTRIBUTIONS

Study concepts and design: GA, PS, SP, ED and AB; nanoalgosome *in vitro* studies and data evaluation: GA, SP, PG, MS, AB; *C. elegans* experiments and data evaluation: PS, GZ and ED; gene expression analyses: AN, SC, PC, VL, NA; mice experiments and data evaluation: MW, GA, AB; microalgae cultures and nanoalgosome isolation and characterization: GA, SP, PG, DPR, AP, ER, SR, VL, PC, CA, NT, RN and MM; manuscript preparation: GA, PS, SP, AB, and ED; approval of the final version of the manuscript submitted: all authors.